

A Coiflet Wavelet Homotopy Technique for Nonlinear PDEs: Application to the Extreme Bending of Orthotropic Plate with Forced Boundary Constraints

Qiang Yu^{1,*}, Shuaimin Wang¹, Junfeng Xiao¹ and Hang Xu²

¹ College of Ocean Science and Engineering, Shanghai Maritime University, Shanghai 201306, China

² School of Naval Architecture Ocean and Civil Engineering, Shanghai Jiao Tong University, Shanghai 200240, China

Received 9 August 2022; Accepted (in revised version) 26 September 2022

Abstract. A generalized homotopy-based Coiflet-type wavelet method for solving strongly nonlinear PDEs with nonhomogeneous edges is proposed. Based on the improvement of boundary difference order by Taylor expansion, the accuracy in wavelet approximation is largely improved and the accumulated error on boundary is successfully suppressed in application. A unified high-precision wavelet approximation scheme is formulated for inhomogeneous boundaries involved in generalized Neumann, Robin and Cauchy types, which overcomes the shortcomings of accuracy loss in homogenizing process by variable substitution. Large deflection bending analysis of orthotropic plate with forced boundary moments and rotations on nonlinear foundation is used as an example to illustrate the wavelet approach, while the obtained solutions for lateral deflection at both small and large deformed stage have been validated compared to the published results in good accuracy. Compared to the other homotopy-based approach, the wavelet scheme possesses good efficiency in transforming the differential operations into algebraic ones by converting the differential operators into iterative matrices, while nonhomogeneous boundary is directly approached dispensing with homogenization. The auxiliary linear operator determined by linear component of original governing equation demonstrates excellent approaching precision and the convergence can be ensured by iterative approach.

AMS subject classifications: 65M10, 78A48

Key words: Wavelet method, higher-order interpolating continuation, homotopy analysis method, geometric nonlinearity, orthotropic plate.

*Corresponding author.
Email: yuqiang@shmtu.edu.cn (Q. Yu)

1 Introduction

To obtain high-precision solution for nonlinear differential equations with inhomogeneous boundaries has been a critical issue in quantitative analysis of science and engineering, which is of great significance in developing effective approaches. Many numerical techniques have been proposed and can be classified into global and local techniques, with the former involving the derivatives of all points in the whole discrete domain, such as Fourier and Chebyshev spectral method [1], Discontinuous Galerkin [2], spectral element methods [3], spectral volume and difference method [4], while the local strategies obtain derivatives in terms of adjacent element, such as Finite Difference Method [5], Finite Element Method [6], Finite Volume Method [7], Boundary Element Method [8].

Homotopy Analysis Method (HAM) [9] has been an analytical powerful technique for dealing with strongly nonlinear problems, due to its freedom in selection of basis by leveraging the convergence properties in developing new numerical schemes. Von Gorder [10] has combined the Fourier method and the HAM to solve the large deflection of thin Kármán plate based on orthogonally sinusoidal basis in good agreement with exact solutions. Mosta et al. [11, 12] have formulated Spectral Homotopy Analysis Method (SHAM) by introducing Chebyshev and Legendre basis in the framework, which successfully overcome the limitations of initial guess and prove the convergence in Sobolev Spaces. Cullen and Clarke [13] have constructed Gegenbauer orthogonal basis expanding Chebyshev polynomials by Schmidt orthogonalization and proposed a fast and highly accurate Gegenbauer Homotopy Analysis Method, with the iterative matrix converted into sparse banded one up to machine precision, while the matrices of collocation points based on Chebyshev differential operators occupy large computational memory resource.

As a bright pearl of modern functional mathematics, wavelet [14, 15] has been an efficient tool in solving partial differential equations, due to its significant superiority on localized analysis. Early research on wavelet can be dated back to an orthogonal compactly supported Haar wavelet [16], which has been subsequently developed by many investigators [17–20]. Sweldens et al. [21, 22] have constructed a flexible wavelet lifting scheme [23], which are not necessarily the translates and dilates of one fixed function dependent of Fourier transformation. Dohono et al. [24–27] have applied a series of directional wavelets to study the characteristics of higher dimensional space introduced into multi-scale geometric analysis, such as Curvelets, Wedgelets, Ridgelets, Contourlets. Similar to early research all independent in various fields, present research of wavelet has not been formed a relatively unified framework and still in the process of exploration.

Many wavelet numerical methods [28–30] have been developed in solving differential equation, firstly studied by Qian and Weiss [31], which are in turn broadly categorised into single scale wavelet and adaptive methods, with the former indicating applying scaling function directly as basis in traditional methods, such as wavelet Galerkin method [32], wavelet collocation method [33], wavelet finite element method [34], closed wavelet method [35], wavelet multi-resolution interpolation Galerkin method [36, 37],

while adaptive methods involves multi-levels wavelet technique by searching a stable and accurate interpolation operator at the intersection of different grids, such as adaptive multi-resolution method [38] and wavelet optimized adaptive method [39].

The compactly supported Coiflet-type wavelet proposed by Coifman et al. [40] was a recently developed orthogonal wavelet base with scaling and wavelet functions both possessing vanishing moments. Tian [41] has constructed the orthogonal and biorthogonal Coiflets system by adding wavelet vanishing moment of odd orders. Wei et al. [42, 43] have formulated the Generalized Orthogonal Coiflets system by substituting scaling function with nonzero-centered vanishing moments into zero-centered ones. Wang et al. [35, 44, 45] have improved the value of first-order vanishing moment of Generalized Orthogonal Coiflets and proposed an effective closed wavelet method for nonlinear problems. Yang and Liao [46,47] have applied the Coiflets in the framework of Homotopy Analysis Method successfully solved the Bratu equation. Yu et al. [48] have developed a homotopy-based Coiflet-type wavelet method to study the pure laminar cavity flow [49], mixed convection flow [50] and double-diffusive nanofluid flow [51].

To deal with nonlinear problems on bounded interval by wavelet approximation, modification of basis is indispensable with various boundary continuations so as to improve the approaching accuracy. The employed zero continuation brings Gibbs' phenomenon [52] involving discontinuous derivatives at boundary points, which results in larger coefficients of wavelet basis and unnecessary computations of refined scales. Periodic continuation [53,54] is to extend the interval length of compactly supported wavelets periodically over the whole real line, only effective in treatment of periodic boundary conditions but invalid for more generalized types. Conformation of interpolated continuation by Spline wavelet has been made by Chui et al. [55], while the interval wavelet describing boundary conditions precisely has been constructed by Daubechies [56] where the complementary boundary wavelets depend on problems needed repeated construction leading to difficulties in numerical implementation.

In views of boundary treatment of Coiflet-type wavelet in former work [35,46,47,57], the third-order difference strategy is valid effective for low-order differential equation with satisfactory precision, but not applicable for higher-order or higher-dimensional nonhomogeneous problems, which greatly restricts its application. Moreover, the previous work [35, 46, 47] mainly focuses on the nonlinear problems with Dirichlet or homogeneous Neumann boundary, while the wavelet strategy is inadequate in dealing with inhomogeneous boundary conditions especially with higher-order derivatives. In addition, selections of convergence control parameter and auxiliary linear operator [46, 47] are based on advanced trial calculation lack of an effective approach to guide how to determine an appropriate one to optimize the convergent process.

In this paper, based on the improvement of boundary difference order by Taylor expansion, a generalized wavelet improvement strategy is developed to suppress the boundary approaching error in application of Coiflet-type wavelet. A unified high-precision wavelet approximation scheme is formulated for inhomogeneous boundaries involving in generalized nonhomogeneous Neumann, Robin and Cauchy types, which

overcomes the shortcomings of accuracy loss in homogenization. A unified homotopy-based wavelet method for nonlinear partial differential equation with nonhomogeneous boundaries is proposed by illustrating the large deflection bending of orthotropic plate with forced boundary moments and rotations on nonlinear elastic foundation as an example.

The paper is illustrated as follows. In Section 2, the wavelet improvement strategy is formulated and the unified approaching scheme is demonstrated. In Section 3, the detailed implementation of homotopy-based wavelet approach for nonlinear PDEs with nonhomogeneous boundary is proposed. Application by nonlinear bending of orthotropic plate with forced boundary restraints is given in Section 4. In Section 5, numerical validation has been made and convergence by iteration are investigated. Some conclusions are made in Section 5.

2 Wavelet improvement strategy

2.1 Construction of Coiflet-type wavelet approximation

A multi-resolution analysis at interval $[a, b]$ by generalized orthogonal Coiflets [35] is constructed by a sequence of orthogonally hierarchical subspaces as

$$0 \subset \cdots \subset \mathbf{V}_0 \subset \mathbf{V}_1 \subset \cdots \subset \mathbf{V}_j \subset \mathbf{V}_{j+1} \subset \cdots \subset L^2[a, b], \quad \mathbf{V}_{j+1} = \mathbf{V}_j \oplus \mathbf{W}_j, \quad (2.1)$$

where $x = a, b$ are the boundary points,

$$\mathbf{V}_j = \text{Span}\{\phi_{j,k} = 2^{\frac{j}{2}}\phi(2^j x - k)\}_{k \in \mathbf{Z}} \quad \text{and} \quad \mathbf{W}_j = \text{Span}\{\psi_{j,k}(x) = 2^{\frac{j}{2}}\psi(2^j x - k)\}_{k \in \mathbf{Z}}$$

are the nested subspaces of square-integrable space $L^2[a, b]$, j is the wavelet resolution level.

The scaling and wavelet functions $\phi(x)$, $\psi(x)$ are localized and smooth governed by a set of coefficients formulated by dual-scale equations as

$$\phi(x) = \sum_{\bar{k}=0}^{L-1} p_{\bar{k}}\phi(2x - \bar{k}), \quad \psi(x) = \sum_{\bar{k}=0}^{L-1} (-1)^{\bar{k}} p_{L-1-\bar{k}}\phi(2x - \bar{k}), \quad (2.2)$$

where L is the compactly supported branch length, $p_{\bar{k}}$ is the low-pass filtering coefficient.

Distinguished from Daubechies wavelet, the scaling and wavelet functions of generalized orthogonal Coiflets possess the properties of vanishing moment as

$$\int_{-\infty}^{+\infty} (x - \mathbf{M}_1)^i \phi(x) dx = \delta_{0,i}, \quad i = 0, \dots, \mathbf{N} - 1, \quad (2.3a)$$

$$\int_{-\infty}^{+\infty} x^i \psi(x) dx = 0, \quad i = 0, \dots, \mathbf{N} - 1, \quad (2.3b)$$

where \mathbf{M}_1 is the first-order moment, $\mathbf{N} = \mathbf{L}/3$ is the order of vanishing moment.

To consider an arbitrary function $f(x) \in \mathbf{L}^2(\mathbf{R})$ approached by the Coiflets at interval I_k^j as

$$f(x) \approx \mathbf{P}^j f(x) = \sum_k c_{j,k} \phi_{j,k}(x), \quad x \in I_k^j = \left[\frac{k}{2^j}, \frac{k+\mathbf{L}-1}{2^j} \right], \tag{2.4}$$

where \mathbf{P}^j is the projective operator, the coefficients $c_{j,k}$ by inner product is

$$c_{j,k} = \int_{I_k^j} f(x) \phi_{j,k}(x) dx. \tag{2.5}$$

The \mathbf{N} th order Taylor expansion at x_0 with $\xi \in [x_0, x]$ is employed as

$$f(x) = \sum_{m=0}^{\mathbf{N}-1} \frac{f^{(m)}(x_0)}{m!} (x-x_0)^m + \frac{f^{(\mathbf{N})}(\xi)}{\mathbf{N}!} (x-x_0)^{\mathbf{N}}, \quad x_0 = \frac{k+\mathbf{M}_1}{2^j}. \tag{2.6}$$

By substituting Eq. (2.6) with respect to Eq. (2.3a), Eq. (2.5) is simplified as

$$c_{j,k} = \sum_{m=0}^{\mathbf{N}-1} \frac{1}{m!} f^{(m)} \left(\frac{k+\mathbf{M}_1}{2^j} \right) \mathbf{A}_m + \frac{f^{(\mathbf{N})}(\xi)}{\mathbf{N}!} \mathbf{A}_{\mathbf{N}}, \quad m=0, \dots, \mathbf{N}, \tag{2.7}$$

where

$$\begin{aligned} \mathbf{A}_m &= \int_{\frac{k}{2^j}}^{\frac{k+\mathbf{L}-1}{2^j}} \left(x - \frac{k+\mathbf{M}_1}{2^j} \right)^m \phi_{j,k}(x) dx \\ &= 2^{-j(\frac{1}{2}+m)} \int_0^{\mathbf{L}-1} (z-\mathbf{M}_1)^m \phi(z) dz = 0, \quad m=1, \dots, \mathbf{N}-1. \end{aligned} \tag{2.8}$$

Then $c_{j,k}$ can be reduced to

$$c_{j,k} = 2^{-\frac{j}{2}} f \left(\frac{k+\mathbf{M}_1}{2^j} \right) + 2^{-j(\frac{1}{2}+\mathbf{N})} \frac{f^{(\mathbf{N})}(\xi)}{\mathbf{N}!} \int_0^{\mathbf{L}-1} (z-\mathbf{M}_1)^{\mathbf{N}} \phi(z) dz, \tag{2.9}$$

with error estimation as

$$\left| c_{j,k} - 2^{-\frac{j}{2}} f \left(\frac{k+\mathbf{M}_1}{2^j} \right) \right| \leq C_0 2^{-j(\frac{1}{2}+\mathbf{N})}, \tag{2.10}$$

where constant C_0 is

$$C_0 = \frac{|f^{(\mathbf{N})}(\xi)|_{\max}}{\mathbf{N}!} \int_0^{\mathbf{L}-1} |z-\mathbf{M}_1|^{\mathbf{N}} \phi(z) dz. \tag{2.11}$$

With substitution of Eq. (2.9), wavelet expansion of Eq. (2.4) is behaved as

$$f(x) \approx \mathbf{P}^j f(x) = \sum_{k=2^j a - 3\mathbf{N} + 2}^{2^j b - 1} f \left(\frac{k+\mathbf{M}_1}{2^j} \right) \phi(2^j x - k), \quad x \in [a, b], \tag{2.12}$$

which can be reformulated by the transformation $k' = k + \mathbf{M}_1$ as

$$f(x) \approx \mathbf{P}^j f(x) = \sum_{k'=2^j a - 3\mathbf{N} + 2 + \mathbf{M}_1}^{2^j b - 1 + \mathbf{M}_1} f\left(\frac{k'}{2^j}\right) \phi(2^j x - k' + \mathbf{M}_1), \tag{2.13}$$

with the restriction as $2^j a, 2^j b$ should be integers.

2.2 Generalized boundary interpolation extension

To overcome the accumulated errors in boundary approximation of Coiflet-type wavelet, a higher order and generalized wavelet boundary difference strategy is constructed in application. As the values of approaching function $f(x)$ in Eq. (2.13) are unknown at intervals $[a - \frac{3\mathbf{N} - 2 - \mathbf{M}_1}{2^j}, a)$ and $(b, b + \frac{\mathbf{M}_1 - 1}{2^j}]$, generalized interpolating continuation by inner difference is employed as

$$f(x) = \begin{cases} \sum_{i=0}^{\mathbf{I}_{tp}} \frac{d_{a,i}}{i!} (x-a)^i, & x < a, \\ f(x), & x \in [a, b], \\ \sum_{i=0}^{\mathbf{I}_{tp}} \frac{d_{b,i}}{i!} (x-b)^i, & x > b, \end{cases} \tag{2.14}$$

where \mathbf{I}_{tp} is the interpolating order, $d_{a,i}, d_{b,i}$ are the coefficients of difference. On the basis of the \mathbf{I}_{tp} th Taylor expansion of $f(x)$ at $x_0 = a, b$ as

$$f(x) = \sum_{i=0}^{\mathbf{I}_{tp}} \frac{f^{(i)}(a)}{i!} (x-a)^i + o[(x-a)^{\mathbf{I}_{tp}}], \quad x = a + \frac{k}{2^j}, \quad k = 0 \sim \mathbf{I}_{tp}, \tag{2.15a}$$

$$f(x) = \sum_{i=0}^{\mathbf{I}_{tp}} \frac{f^{(i)}(b)}{i!} (x-b)^i + o[(x-b)^{\mathbf{I}_{tp}}], \quad x = b - \frac{k}{2^j}, \quad k = 0 \sim \mathbf{I}_{tp}, \tag{2.15b}$$

the difference equations in matrix form are obtained by

$$[\mathbf{C}_a]_{\mathbf{I}_{tp} \times 1} = [\mathbf{Q}_a]_{\mathbf{I}_{tp} \times 1} [\mathbf{D}_a]_{\mathbf{I}_{tp} \times \mathbf{I}_{tp}}, \quad [\mathbf{C}_b]_{\mathbf{I}_{tp} \times 1} = [\mathbf{Q}_b]_{\mathbf{I}_{tp} \times 1} [\mathbf{D}_b]_{\mathbf{I}_{tp} \times \mathbf{I}_{tp}}, \tag{2.16}$$

where $\mathbf{C}_a = [f_{j,2^j a+k} = f(a+k/2^j)]$, $\mathbf{C}_b = [f_{j,2^j b-k} = f(b-k/2^j)]$ are the matrices of unknown values at boundary interpolation points, $\mathbf{D}_a = [f^{(i)}(a)]$, $\mathbf{D}_b = [f^{(i)}(b)]$ are the matrices of boundary derivatives, $\mathbf{Q}_a = [q_{a,k,i}]$, $\mathbf{Q}_b = [q_{b,k,i}]$ are the matrices by Taylor expansion as

$$q_{a,k,i} = \frac{k^i}{i!} \frac{1}{2^{ij}}, \quad q_{b,k,i} = (-1)^i q_{a,k,i}, \quad k, i = 0 \sim \mathbf{I}_{tp}. \tag{2.17}$$

Owing to $\mathbf{Q}_a, \mathbf{Q}_b$ are square and full of rank, their inverses $\mathbf{P}_a, \mathbf{P}_b$ can be expressed as

$$\mathbf{P}_a = \mathbf{Q}_a^{-1} = [2^{-ij} p_{a,i,k}]_{\mathbf{I}_{tp} \times \mathbf{I}_{tp}}, \quad \mathbf{P}_b = \mathbf{Q}_b^{-1} = [2^{-ij} p_{b,i,k}]_{\mathbf{I}_{tp} \times \mathbf{I}_{tp}}, \tag{2.18}$$

where the difference matrices $\hat{\mathbf{P}}_a, \hat{\mathbf{P}}_b$ at $\mathbf{I}_{tp} = 5$ are

$$\hat{\mathbf{P}}_a = [p_{a,i,k}] = \begin{pmatrix} 1 & 0 & 0 & 0 & 0 & 0 \\ -\frac{137}{60} & 5 & -5 & \frac{10}{3} & -\frac{5}{4} & \frac{1}{5} \\ \frac{15}{4} & -\frac{77}{6} & \frac{107}{6} & -13 & \frac{61}{12} & -\frac{5}{6} \\ \frac{17}{4} & \frac{71}{4} & \frac{59}{2} & \frac{49}{2} & \frac{41}{4} & \frac{7}{4} \\ 3 & -14 & 26 & -24 & 11 & -2 \\ -1 & 5 & -10 & 10 & -5 & 1 \end{pmatrix}, \tag{2.19a}$$

$$\hat{\mathbf{P}}_b = [p_{b,i,k}] = \begin{pmatrix} 1 & 0 & 0 & 0 & 0 & 0 \\ \frac{137}{60} & -5 & 5 & -\frac{10}{3} & \frac{5}{4} & -\frac{1}{5} \\ \frac{15}{4} & -\frac{77}{6} & \frac{107}{6} & -13 & \frac{61}{12} & -\frac{5}{6} \\ \frac{17}{4} & \frac{71}{4} & \frac{59}{2} & \frac{49}{2} & \frac{41}{4} & \frac{7}{4} \\ \frac{4}{4} & -\frac{4}{4} & \frac{2}{2} & -\frac{2}{2} & \frac{4}{4} & -\frac{4}{4} \\ 3 & -14 & 26 & -24 & 11 & -2 \\ 1 & -5 & 10 & -10 & 5 & -1 \end{pmatrix}. \tag{2.19b}$$

Then the coefficients $d_{a,i}, d_{b,i}$ in Eq. (2.14) can be further rewritten as

$$d_{a,i} = \sum_{k=0}^{\mathbf{I}_{tp}} p_{a,i,k} f_{j,2^j a+k}, \quad d_{b,i} = \sum_{k=0}^{\mathbf{I}_{tp}} p_{b,i,k} f_{j,2^j b-k}, \tag{2.20}$$

with Eq. (2.20) denoted as

$$f(x) = \begin{cases} \sum_{k=0}^{\mathbf{I}_{tp}} f_{j,2^j a+k} T_{a,k}(x), & x < a, \\ f(x), & x \in [a,b], \\ \sum_{k=0}^{\mathbf{I}_{tp}} f_{j,2^j b-k} T_{b,k}(x), & x > b, \end{cases} \tag{2.21}$$

where the boundary interpolating functions $T_{a,k}(x), T_{b,k}(x)$ are

$$T_{a,k}(x) = \sum_{i=0}^{\mathbf{I}_{tp}} \frac{p_{a,i,k}}{i!} (x-a)^i, \quad T_{b,k}(x) = \sum_{i=0}^{\mathbf{I}_{tp}} \frac{p_{b,i,k}}{i!} (x-b)^i. \tag{2.22}$$

With substitution of Eq. (2.21) into Eq. (2.13), the wavelet approximation is reformulated as

$$f(x) \approx \mathbf{P}_{[a,b]}^j f(x) = \sum_{k=2^j a}^{2^j b} f\left(\frac{k}{2^j}\right) \varphi_{j,k}^{[a,b]}(x), \quad x \in [a,b], \tag{2.23}$$

where the Coiflets $\varphi_{j,k}^{[a,b]}(x)$ with modified interpolating continuation is

$$\varphi_{j,k}^{[a,b]}(x) = \begin{cases} \sum_{i=2^j a - 3N + 2 + \mathbf{M}_1}^{2^j a - 1} T_{a,k-2^j a} \left(\frac{i}{2^j} \right) \phi_{j,i} + \phi_{j,k}, & k \in [2^j a, 2^j a + \mathbf{I}_{tp}], \\ \phi_{j,k}, & k \in [2^j a + \mathbf{I}_{tp} + 1, 2^j b - \mathbf{I}_{tp} - 1], \\ \sum_{i=2^j b + 1}^{2^j b - 1 + \mathbf{M}_1} T_{b,2^j b - k} \left(\frac{i}{2^j} \right) \phi_{j,i} + \phi_{j,k}, & k \in [2^j b - \mathbf{I}_{tp}, 2^j b], \end{cases} \quad (2.24)$$

in which

$$\phi_{j,k}(x) = \phi(2^j x - k + \mathbf{M}_1), \quad \phi_{j,i}(x) = \phi(2^j x - i + \mathbf{M}_1).$$

In addition, operator \mathcal{R} acting on $f(x)$ can be transformed on the approaching basis as

$$\mathcal{R}[f(x)] \approx \mathcal{R}[\mathbf{P}_{[a,b]}^j f(x)] = \sum_{k=2^j a}^{2^j b} f\left(\frac{k}{2^j}\right) \mathcal{R}[\varphi_{j,k}(x)], \quad R = \mathcal{L}, \mathcal{N}, \quad (2.25)$$

where \mathcal{L}, \mathcal{N} are the linear and nonlinear operators, respectively.

To validate the approaching accuracy of Eq. (2.23) by improving the difference order \mathbf{I}_{tp} , the overall absolute error $\|E_f\|_1$ and mean square error $\|E_f\|_2$ are formulated as

$$\|E_f\|_1 = \int_a^b E_f dx \approx \frac{1}{N_j} \sum_{k=2^j a}^{2^j b} \left| f\left(\frac{k}{2^j}\right) - f_e\left(\frac{k}{2^j}\right) \right|, \quad (2.26a)$$

$$\|E_f\|_2 = \left[\int_a^b E_f^2 dx \right]^{\frac{1}{2}} \approx \frac{1}{N_j} \sqrt{\sum_{k=2^j a}^{2^j b} \left[f\left(\frac{k}{2^j}\right) - f_e\left(\frac{k}{2^j}\right) \right]^2}, \quad (2.26b)$$

in which the error distributed function Err_f is

$$E_f = |f(x) - f_e(x)|, \quad x \in [a, b], \quad (2.27)$$

where $N_j = 2^j(b - a) + 1$ is the number of dyadic points, $f(x)$ and $f_e(x)$ are the calculated and exact solutions.

As showed in Table 1, the absolute error $\|E_f\|_1$ and mean square error $\|E_f\|_2$ of derivatives at different orders and single integration of test function $f(x) = \sin(x)$ are elaborated at wavelet resolution level $j = 8$. By the improvement of boundary difference order \mathbf{I}_{tp} , the global errors gradually decline and all converge to a constant magnitude when $\mathbf{I}_{tp} \geq 5$, which reveals the approaching precision is largely improved and further validates the effectiveness of the wavelet strategy. Besides, it can be found that differential operation by wavelet approximation results in certain accuracy loss, while the integral operation is conducive to the improvement of approaching precision.

Table 1: Absolute errors $\|E_f\|_1$ and mean square errors $\|E_f\|_2$ of derivatives and first integration of test function $f(x) = \sin(x)$ by improving boundary interpolating order $I_{tp} = 1 \sim 8$ at wavelet resolution level $j = 8$.

	I_{tp}	$f'(x)$	$f''(x)$	$f'''(x)$	$f^{(4)}(x)$	$\theta(x) = \int_0^x f(z) dz$
$\ E_f\ _1$	1	3.72849786E-07	1.66492005E-03	1.46153183E-01	3.49298562E+01	3.66460816E-11
	2	1.53779050E-06	3.10423722E-03	4.06624956E-01	5.98299301E+01	1.68219847E-10
	3	2.25883288E-10	4.86297576E-07	7.06245775E-05	1.33350147E-02	2.52028420E-14
	4	1.52296806E-10	3.20280054E-07	8.30486538E-05	4.10317567E-02	1.55138257E-14
	5	3.71212441E-12	1.00235707E-07	4.10639271E-06	7.26396972E-03	1.08993341E-17
	6	3.68760445E-12	1.00348172E-07	4.09701866E-06	7.26930974E-03	1.51591026E-17
	7	3.67465529E-12	1.00244960E-07	4.08506979E-06	7.25725395E-03	1.43786107E-17
	8	3.67466296E-12	1.00244928E-07	4.08506325E-06	7.25725125E-03	1.43786811E-17
$\ E_f\ _2$	1	2.31148631E-07	8.75704429E-04	8.94226605E-02	1.82842514E+01	2.31006303E-12
	2	8.56149898E-07	1.34336684E-03	2.04901705E-01	2.54620122E+01	1.05431881E-11
	3	1.22529771E-10	1.64585474E-07	3.40285997E-05	2.96676449E-03	1.57878809E-15
	4	8.11117873E-11	1.04734132E-07	4.56807608E-05	1.52161165E-02	9.71885409E-16
	5	2.55992713E-13	6.95886803E-09	2.83930238E-07	5.03820891E-04	7.84702793E-19
	6	2.55221623E-13	6.95911611E-09	2.83673187E-07	5.03840040E-04	1.04247197E-18
	7	2.55073309E-13	6.95887635E-09	2.83567735E-07	5.03796338E-04	9.99124868E-19
	8	2.55073319E-13	6.95887629E-09	2.83567729E-07	5.03796334E-04	9.99128718E-19

2.3 Strategy for nonhomogeneous linear boundaries

2.3.1 Dirichlet boundary

To consider a linear Dirichlet boundary where μ_a, μ_b are constant as

$$f(a) = \mu_a, \quad f(b) = \mu_b, \tag{2.28}$$

the Coiflet-type wavelet expansion of $f(x)$ is elaborated by

$$f(x) \approx \mathbf{P}_{[a,b]}^j f(x) = \sum_{k'=2^j a+1}^{2^j b-1} f\left(\frac{k'}{2^j}\right) \varphi_{j,k'}(x) + \mu_a \varphi_{j,2^j a}(x) + \mu_b \varphi_{j,2^j b}(x), \tag{2.29}$$

while its derivatives with respect to the Eq. (2.25) is employed as

$$f^{(n)}(x) \approx \sum_{k'=2^j a+1}^{2^j b-1} f\left(\frac{k'}{2^j}\right) \varphi_{j,k'}^{(n)}(x) + \mu_a \varphi_{j,2^j a}^{(n)}(x) + \mu_b \varphi_{j,2^j b}^{(n)}(x), \quad \mathbf{n} \geq 1, \tag{2.30}$$

where \mathbf{n} is the differential order.

2.3.2 Generalized Neumann boundary

If subjects to the generalized Neumann-type boundaries, higher-order derivatives of $f(x)$ on boundaries are in advance given by

$$\left. \frac{d^\alpha f(x)}{dx^\alpha} \right|_{x=a} = v_{a,\alpha}, \quad \left. \frac{d^\beta f(x)}{dx^\beta} \right|_{x=b} = v_{b,\beta}, \tag{2.31}$$

where $\alpha, \beta \geq 1$ are the boundary differential orders, $\nu_{a,\alpha}, \nu_{b,\beta}$ are constants.

To attach the inhomogeneous values, difference coefficients in Eq. (2.20) are substituted by

$$d_{a,i} = \sum_{k=0}^{I_{tp}} p_{a,i,k} f_{j,2^i a+k} (1 - \delta_{i,\alpha}) + \delta_{i,\alpha} \nu_{a,\alpha}, \tag{2.32a}$$

$$d_{b,i} = \sum_{k=0}^{I_{tp}} p_{b,i,k} f_{j,2^i b-k} (1 - \delta_{i,\beta}) + \delta_{i,\beta} \nu_{b,\beta}, \tag{2.32b}$$

where $\delta_{i,k}$ is the Kronecker operator. Eq. (2.21) is renewed as

$$f(x) = \begin{cases} \sum_{k=0}^{I_{tp}} [f_{j,2^i a+k} T_{a,k}^N(x) + \delta_{k,\alpha} \frac{\nu_{a,\alpha}}{k!} (x-a)^k], & x < a, \\ f(x), & x \in [a, b], \\ \sum_{k=0}^{I_{tp}} [f_{j,2^i b-k} T_{b,k}^N(x) + \delta_{k,\beta} \frac{\nu_{b,\beta}}{k!} (x-b)^k], & x > b, \end{cases} \tag{2.33}$$

and the interpolating functions $T_{a,k}^N(x), T_{b,k}^N(x)$ for Neumann type are

$$T_{a,k}^N(x) = \sum_{i=0}^{I_{tp}} \frac{p_{a,i,k}}{i!} (x-a)^i (1 - \delta_{i,\alpha}), \tag{2.34a}$$

$$T_{b,k}^N(x) = \sum_{i=0}^{I_{tp}} \frac{p_{b,i,k}}{i!} (x-b)^i (1 - \delta_{i,\beta}). \tag{2.34b}$$

Substituting Eq. (2.33) into Eq. (2.13), it can be obtained by

$$f(x) = \sum_{i=2^j a-3N+2+M_1}^{2^j a-1} \sum_{k=0}^{I_{tp}} \left[f_{j,2^i a+k} T_{a,k}^N \left(\frac{i}{2^j} \right) \phi_{j,k}(x) + \delta_{k,\alpha} \frac{\nu_{a,\alpha}}{k!} (x-a)^k \right] + \sum_{k=2^j a}^{2^j b} f_{j,k} \phi_{j,k}(x) \\ + \sum_{i=2^j b+1}^{2^j b-1+M_1} \sum_{k=0}^{I_{tp}} \left[f_{j,2^i b-k} T_{b,k}^N(x) \left(\frac{i}{2^j} \right) \phi_{j,k}(x) + \delta_{k,\beta} \frac{\nu_{b,\beta}}{k!} (x-b)^k \right]. \tag{2.35}$$

By exchanging summation orders, it is behaved as

$$f(x) = \left\{ \begin{aligned} & \sum_{k=2^j a}^{2^j a + \mathbf{I}_{tp}} f_{j,k} \left\{ \sum_{i=2^j a - 3\mathbf{N} + 2 + \mathbf{M}_1}^{2^j a - 1} T_{a,k-2^j a}^{\mathbf{N}} \left(\frac{i}{2^j} \right) \phi_{j,i} + \phi_{j,k} \right\} \\ & + v_{a,\alpha} \sum_{i=2^j a - 3\mathbf{N} + 2 + \mathbf{M}_1}^{2^j a - 1} \frac{(x-a)^\alpha}{\alpha!} \phi_{j,i}, \quad k \in [2^j a, 2^j a + \mathbf{I}_{tp}], \\ & + \sum_{k=2^j a + \mathbf{I}_{tp} + 1}^{2^j b - \mathbf{I}_{tp} - 1} f_{j,k} \phi_{j,k}, \quad k \in [2^j a + \mathbf{I}_{tp} + 1, 2^j b - \mathbf{I}_{tp} - 1], \\ & + \sum_{k=2^j b - \mathbf{I}_{tp}}^{2^j b} f_{j,k} \left\{ \sum_{i=2^j b + 1}^{2^j b - 1 + \mathbf{M}_1} T_{b,2^j b - k}^{\mathbf{N}} \left(\frac{i}{2^j} \right) \phi_{j,i} + \phi_{j,k} \right\} \\ & + v_{b,\beta} \sum_{i=2^j b + 1}^{2^j b - 1 + \mathbf{M}_1} \frac{(x-b)^\beta}{\beta!} \phi_{j,i}, \quad k \in [2^j b - \mathbf{I}_{tp}, 2^j b]. \end{aligned} \right. \quad (2.36)$$

Finally, wavelet expansion of $f(x)$ with nonhomogeneous Neumann-type edges in Eq. (2.31) is employed as

$$f(x) \approx \mathbf{P}_{[a,b]}^j f(x) = \sum_{k=2^j a}^{2^j b} f \left(\frac{k}{2^j} \right) h_{j,k}(x) + v_{a,\alpha} \omega_{j,\alpha}^a(x) + v_{a,\beta} \omega_{j,\beta}^b(x), \quad (2.37)$$

with its derivatives with respect to Eq. (2.25) employed as

$$f^{(\mathbf{n})}(x) \approx \sum_{k=2^j a}^{2^j b} f \left(\frac{k}{2^j} \right) h_{j,k}^{(\mathbf{n})}(x) + v_{a,\alpha} \omega_{j,\alpha}^{a,(\mathbf{n})} + v_{a,\beta} \omega_{j,\beta}^{b,(\mathbf{n})}, \quad \mathbf{n} \geq 1, \quad (2.38)$$

where the modified Coiflet-type wavelet $h_{j,k}(x)$ at interval $[a, b]$ is

$$h_{j,k}(x) = \varphi_{j,k}^{[a,b]}(x) \Big|_{T_{a,k}(x) \rightarrow T_{a,k}^{\mathbf{N}}(x), T_{b,k}(x) \rightarrow T_{b,k}^{\mathbf{N}}(x)}. \quad (2.39)$$

Particularly, boundary Coiflets $\omega_{j,\alpha}^a, \omega_{j,\beta}^b$ at $x = a, b$ corresponding to the nonhomogeneous information are

$$\omega_{j,\alpha}^a = \sum_{i=2^j a - 3\mathbf{N} + 2 + \mathbf{M}_1}^{2^j a - 1} \frac{(x-a)^\alpha}{\alpha!} \phi_{j,i}, \quad (2.40a)$$

$$\omega_{j,\beta}^b = \sum_{i=2^j b + 1}^{2^j b - 1 + \mathbf{M}_1} \frac{(x-b)^\beta}{\beta!} \phi_{j,i}, \quad (2.40b)$$

which are determined by the orders of boundary derivatives.

2.3.3 Generalized Robin boundary

The nonhomogeneous Robin-type boundary is a specification of a linear combination of $f(x)$ and its higher-order derivatives at both sides as

$$\left[\frac{d^\alpha f(x)}{dx^\alpha} + \gamma_a f(x) \right] \Big|_{x=a} = v_{a,\alpha}, \quad \left[\frac{d^\beta f(x)}{dx^\beta} + \gamma_b f(x) \right] \Big|_{x=b} = v_{b,\beta}, \quad (2.41)$$

where γ_a, γ_b and $v_{a,\alpha}, v_{b,\alpha}$ refer to the constant coefficients and sources.

Since $f(x)$ is bounded on boundaries, Eq. (2.41) can be simplified into

$$\frac{d^\alpha f(x)}{dx^\alpha} \Big|_{x=a} = v_{a,\alpha} - \gamma_a f(a), \quad \frac{d^\beta f(x)}{dx^\beta} \Big|_{x=b} = v_{b,\beta} - \gamma_b f(b). \quad (2.42)$$

Analogously to the Neumann-type strategy thereinbefore, Eq. (2.33) can be substituted by

$$f(x) = \begin{cases} \sum_{k=0}^{I_{tp}} \left[f_{j,2^i a+k} T_{a,k}^N(x) + \delta_{k,\alpha} \frac{v_{a,\alpha} - \gamma_a f(a)}{k!} (x-a)^k \right], & x < a, \\ f(x), & x \in [a, b], \\ \sum_{k=0}^{I_{tp}} \left[f_{j,2^i b-k} T_{b,k}^N(x) + \delta_{k,\beta} \frac{v_{b,\beta} - \gamma_b f(b)}{k!} (x-b)^k \right], & x > b, \end{cases} \quad (2.43)$$

which can be rewritten as

$$f(x) = \begin{cases} \sum_{k=0}^{I_{tp}} \left[f_{j,2^i a+k} T_{a,k}^B(x) + \delta_{k,\alpha} \frac{v_{a,\alpha}}{k!} (x-a)^k \right], & x < a, \\ f(x), & x \in [a, b], \\ \sum_{k=0}^{I_{tp}} \left[f_{j,2^i b-k} T_{b,k}^B(x) + \delta_{k,\beta} \frac{v_{b,\beta}}{k!} (x-b)^k \right], & x > b, \end{cases} \quad (2.44)$$

where interpolating functions $T_{a,k}^B(x), T_{b,k}^B(x)$ for Robin boundary are

$$T_{a,k}^B(x) = \sum_{i=0}^{I_{tp}} \frac{p_{a,i,k}}{i!} (x-a)^i (1 - \delta_{i,\alpha}) - \gamma_a \delta_{0,k} \frac{(x-a)^\alpha}{\alpha!}, \quad (2.45a)$$

$$T_{b,k}^B(x) = \sum_{i=0}^{I_{tp}} \frac{p_{b,i,k}}{i!} (x-b)^i (1 - \delta_{i,\beta}) - \gamma_b \delta_{0,k} \frac{(x-b)^\beta}{\beta!}. \quad (2.45b)$$

Then, wavelet expansion of $f(x)$ subjected to the nonhomogeneous Robin-type edges with respect to Eq. (2.41) is

$$f(x) \approx \mathbf{P}_{[a,b]}^j f(x) = \sum_{k=2^j a}^{2^j b} f\left(\frac{k}{2^j}\right) h_{j,k}(x) + v_{a,\alpha} \omega_{j,\alpha}^a(x) + v_{a,\beta} \omega_{j,\beta}^b(x), \quad (2.46)$$

where

$$h_{j,k}(x) = \varphi_{j,k}^{[a,b]}(x) \Big|_{T_{a,k}(x) \rightarrow T_{a,k}^B(x), T_{b,k}(x) \rightarrow T_{b,k}^B(x)}, \tag{2.47}$$

with its derivatives identical to the formulation of Eq. (2.38).

2.3.4 Generalized Cauchy boundary

Different from Robin boundary, the generalized Cauchy condition specifies both boundary value and its normal derivative of $f(x)$, which imposes aligned Dirichlet and higher-order Neumann conditions as

$$f(a) = \mu_a, \quad f(b) = \mu_b, \quad \left. \frac{d^\alpha f(x)}{dx^\alpha} \right|_{x=a} = \nu_{a,\alpha}, \quad \left. \frac{d^\beta f(x)}{dx^\beta} \right|_{x=b} = \nu_{b,\beta}. \tag{2.48}$$

Combing Eqs. (2.29), (2.37) with respect to Eq. (2.48), wavelet expansion is given as

$$f(x) \approx \mathbf{P}_{[a,b]}^j f(x) = \sum_{k=2^{j_a}+1}^{2^{j_b}-1} f\left(\frac{k}{2^j}\right) h_{j,k}(x) + \mu_a \varphi_{j,2^{j_a}}(x) + \mu_b \varphi_{j,2^{j_b}}(x) + \nu_{a,\alpha} \omega_{j,\alpha}^a(x) + \nu_{a,\beta} \omega_{j,\beta}^b(x), \tag{2.49}$$

where $h_{j,k}(x)$ is chosen the same as Eq. (2.39).

For the hybrid mixed Robin boundary presented as

$$\left. \begin{aligned} f(a) = \mu_a, & \quad f(b) = \mu_b, \\ \left[\frac{d^\alpha f(x)}{dx^\alpha} + \gamma_a f(x) \right] \Big|_{x=a} = \nu_{a,\alpha}, & \quad \left[\frac{d^\beta f(x)}{dx^\beta} + \gamma_b f(x) \right] \Big|_{x=b} = \nu_{b,\beta}, \end{aligned} \right\} \tag{2.50}$$

the corresponding wavelet approximation is identical as the Eq. (2.49) but $h_{j,k}(x)$ should be substituted for Eq. (2.47). Nevertheless, in terms of Eq. (2.42), the Robin ingredient of Eq. (2.50) can be degraded to Neumann-type as

$$\left. \frac{d^\alpha f(x)}{dx^\alpha} \right|_{x=a} = \nu_{a,\alpha} - \gamma_a \mu_a, \quad \left. \frac{d^\beta f(x)}{dx^\beta} \right|_{x=b} = \nu_{b,\beta} - \gamma_b \mu_b. \tag{2.51}$$

The wavelet expansion can be replaced by

$$f(x) \approx \mathbf{P}_{[a,b]}^j f(x) = \sum_{k=2^{j_a}+1}^{2^{j_b}-1} f\left(\frac{k}{2^j}\right) h_{j,k}(x) + \nu_{a,\alpha} \omega_{j,\alpha}^a(x) + \nu_{a,\beta} \omega_{j,\beta}^b(x) + (\nu_{a,\alpha} - \gamma_a \mu_a) \varphi_{j,2^{j_a}}(x) + (\nu_{b,\beta} - \gamma_b \mu_b) \varphi_{j,2^{j_b}}(x), \tag{2.52}$$

where

$$h_{j,k}(x) = \varphi_{j,k}^{[a,b]}(x) \Big|_{T_{a,k}(x) \rightarrow T_{a,k}^N(x), T_{b,k}(x) \rightarrow T_{b,k}^N(x)}. \tag{2.53}$$

2.4 Application in linear ODEs with nonhomogeneous boundaries

To evaluate the numerical accuracy of scheme above, two ordinary differential equations separately subjected to nonhomogeneous Neumann and Robin boundaries are employed as

$$\text{Case I: } \begin{cases} \mathcal{L}_1[u_1(x)] = \frac{d^2u_1(x)}{dx^2} - 2\pi \frac{du_1(x)}{dx} + 2\pi^2 u_1(x) = 0, \\ u_1(x)|_{x=a} = 1, \quad \left. \frac{d^\beta u_1(x)}{dx^\beta} \right|_{x=b} = -1, \end{cases} \quad (2.54a)$$

$$\text{Case II: } \begin{cases} \mathcal{L}_2[u_2(x)] = \frac{d^2u_2(x)}{dx^2} - 2 \frac{du_2(x)}{dx} + 2u_2(x) = 0, \\ \left[\frac{du_2(x)}{dx} - u_2(x) \right] \Big|_{x=a} = 1, \quad \left[\frac{du_2(x)}{dx} - u_2(x) \right] \Big|_{x=b} = -1, \end{cases} \quad (2.54b)$$

with exact solutions as

$$u_{1e}(x) = e^{-\pi(a+b-x)} \cdot \begin{cases} \beta_1(x), & \beta = 1, \\ \beta_2(x), & \beta = 2, \end{cases} \quad (2.55a)$$

$$u_{2e} = -e^{x-a-b} \csc(a-b) [e^a \cos(a-x) + e^b \cos(b-x)], \quad (2.55b)$$

where

$$\beta_1(x) = \frac{e^{\pi a} \sin \pi(a-x) + \pi e^{\pi b} \sin \pi(b-x) + \pi e^{\pi b} \cos \pi(b-x)}{\pi [\cos \pi(a-b) - \sin \pi(a-b)]},$$

$$\beta_2(x) = \frac{e^{\pi a} \sin \pi(a-x) + 2\pi^2 e^{\pi b} \cos \pi(b-x)}{2\pi^2 \cos \pi(a-b)}.$$

Wavelet expansions of u_1, u_2 in consideration of Eq. (2.37) are separately given as

$$u_1(x) \approx \sum_{k'=2^j a+1}^{2^j b} u_1 \left(\frac{k'}{2^j} \right) h_{j,k'}^1(x) + h_{j,2^j a}^1(x) - \omega_{j,\beta}^b, \quad (2.56a)$$

$$u_2(x) \approx \sum_{k=2^j a}^{2^j b} u_2 \left(\frac{k}{2^j} \right) h_{j,k}^2(x) + \omega_{j,1}^a - \omega_{j,1}^b, \quad (2.56b)$$

where the selected Coiflets basis are

$$h_{j,k}^1(x) = \varphi_{j,k}(x) \Big|_{T_{b,k} \rightarrow \tilde{T}_{b,k}}, \quad \hat{T}_{b,k} = \sum_{i=0}^{I_{tp}} \frac{p_{b,i,k}}{i!} (x-b)^i (1-\delta_{i,\beta}),$$

$$h_{j,k}^2(x) = \varphi_{j,k}(x) \Big|_{T_{a,k}(x) \rightarrow \tilde{T}_{a,k}(x), T_{b,k}(x) \rightarrow \tilde{T}_{b,k}(x)},$$

$$\begin{aligned} \tilde{T}_{a,k}(x) &= \sum_{i=0}^{I_p} \frac{p_{a,i,k}}{i!} (x-a)^i (1-\delta_{i,1}) + \delta_{0,k}(x-a), \\ \tilde{T}_{b,k}(x) &= \sum_{i=0}^{I_p} \frac{p_{b,i,k}}{i!} (x-b)^i (1-\delta_{i,1}) + \delta_{0,k}(x-b). \end{aligned}$$

Substituting Eq. (2.56a) into Eq. (2.54a) and Eq. (2.56b) into Eq. (2.54b), we give

$$\sum_{k'=2^j a+1}^{2^j b} u_1 \left(\frac{k'}{2^j} \right) \mathcal{L}_1[h_{j,k'}^1(x)] + \mathcal{L}_1[h_{j,2^j a}^1(x)] - \mathcal{L}_1[\omega_{j,\beta}^b] = 0, \tag{2.57a}$$

$$\sum_{k=2^j a}^{2^j b} u_2 \left(\frac{k}{2^j} \right) \mathcal{L}_2[h_{j,k}^2(x)] + \mathcal{L}_2[\omega_{j,1}^a] - \mathcal{L}_2[\omega_{j,1}^b] = 0. \tag{2.57b}$$

To respectively multiply $h_{j,l'}(x)$, $h_{j,l}(x)$ at both ends of Eq. (2.57a) and Eq. (2.57b), algebra equations are formulated by Galerkin method as

$$\tilde{\mathbf{A}}_i \cdot \hat{\mathbf{U}}_i = -\tilde{\mathbf{B}}_i + \tilde{\mathbf{C}}_i, \quad i = 1, 2, \tag{2.58}$$

where straight vectors and iterating matrices are

$$\begin{aligned} \hat{\mathbf{U}}_1 &= \left\{ u'_k = u_1 \left(\frac{k'}{2^j} \right) \right\}, & \hat{\mathbf{U}}_2 &= \left\{ u_k = u_2 \left(\frac{k}{2^j} \right) \right\}, \\ \tilde{\mathbf{A}}_1^T &= \tilde{\Gamma}_{k',l'}^{j,2} - 2\pi \tilde{\Gamma}_{k',l'}^{j,1} + 2\pi^2 \tilde{\Gamma}_{k',l'}^{j,0}, & \tilde{\mathbf{A}}_2^T &= \tilde{\Gamma}_{k,l}^{j,2} - 2\tilde{\Gamma}_{k,l}^{j,1} + 2\tilde{\Gamma}_{k,l}^{j,0}, \\ \tilde{\mathbf{B}}_1^T &= \tilde{\Gamma}_{2^j a,l'}^{j,2} - 2\pi \tilde{\Gamma}_{2^j a,l'}^{j,1} + 2\pi^2 \tilde{\Gamma}_{2^j a,l'}^{j,0}, & \tilde{\mathbf{B}}_2^T &= \hat{\Gamma}_{L,l}^{j,2} - 2\hat{\Gamma}_{L,l}^{j,1} + 2\hat{\Gamma}_{L,l}^{j,0}, \\ \tilde{\mathbf{C}}_1^T &= \hat{\Gamma}_{R,l'}^{j,2} - 2\pi \hat{\Gamma}_{R,l'}^{j,1} + 2\pi^2 \hat{\Gamma}_{R,l'}^{j,0}, & \tilde{\mathbf{C}}_2^T &= \hat{\Gamma}_{R,l}^{j,2} - 2\hat{\Gamma}_{R,l}^{j,1} + 2\hat{\Gamma}_{R,l}^{j,0}, \\ k', l' &= 2^j a + 1 \sim 2^j b, & k, l &= 2^j a \sim 2^j b. \end{aligned}$$

The connection coefficient by inner product of modified Coiflets $\tilde{\Gamma}_{k,l}^{j,n}$ is

$$\tilde{\Gamma}_{k,l}^{j,n} = \left\{ \gamma_q = \int_a^b \frac{d^n h_{j,k}}{dx^n} h_{j,l} dx \right\}, \quad q = [2^j(b-a) + 1](k - 2^j a) + l - 2^j a + 1, \tag{2.59}$$

which can be computed in view of Eqs. (2.24), (2.40) as

$$\mathbf{Y}_{k,l}^{j,n} = 2^{j(n-1)} [\mathbf{\Lambda}_{k-l}^n (2^j b - l) - \mathbf{\Lambda}_{k-l}^n (2^j a - l)], \tag{2.60}$$

while the calculated algorithms of $\mathbf{\Lambda}_k^n(x)$ can be referred in [58].

The connection coefficients $\hat{\Gamma}_{L,l}^{j,n}$, $\hat{\Gamma}_{R,l}^{j,n}$ composed by inner product of boundary Coiflets with modified Coiflet are given as

$$\hat{\Gamma}_{L,l}^{j,n} = \left\{ \gamma_l = \int_a^b \frac{d^n \omega_{j,\alpha}^a}{dx^n} h_{j,l} dx \right\}, \quad \hat{\Gamma}_{R,l}^{j,n} = \left\{ \gamma_l = \int_a^b \frac{d^n \omega_{j,\beta}^b}{dx^n} h_{j,l} dx \right\}. \tag{2.61}$$

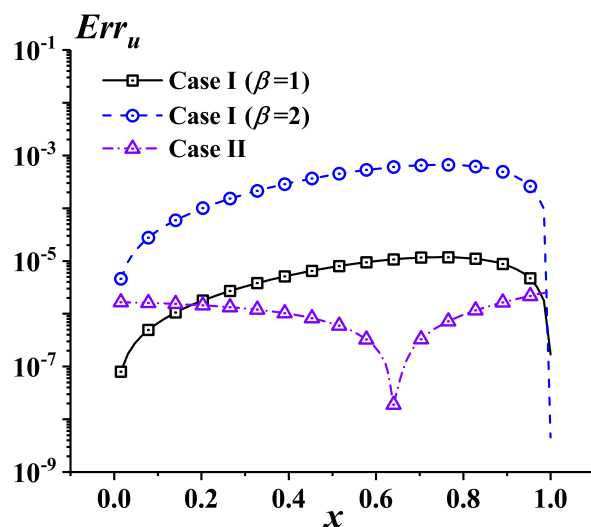


Figure 1: Absolute approaching error distribution of linear PDEs in Case I ($\beta = 1, 2$) and Case II at wavelet resolution level $j = 6$.

As depicted in Fig. 1, distribution of absolute approaching error in linear PDEs of Case I ($\beta = 1, 2$) and Case II at resolution level $j = 6$ are demonstrated, which reveals the wavelet strategy is effective for both nonhomogeneous generalized Neumann and Robin boundaries with satisfactory precision. The global mean square error $\|E_u\|_2$ and CPU time illustrated in Table 2 indicates the approaching accuracy will be improved by adding j but more time consumption is needed. However, due to the accumulation of numerical errors in obtaining inverse of matrix \tilde{A} in Eq. (2.58), the tendency of precision enhancement gradually slows down. To balance the accuracy and efficiency, we select $j = 6$, $I_{tp} = 5$ as appropriate resolution level and reasonable difference order in the calculations thereafter.

Table 2: Mean square error and CPU time consumption in approximation of linear Case I and II at resolution level $j = 3 \sim 9$ when $I_{tp} = 5$.

j	Case I ($\beta = 1$)		Case I ($\beta = 2$)		Case II	
	$\ E_u\ _2$	Time (s)	$\ E_u\ _2$	Time (s)	$\ E_u\ _2$	Time (s)
4	8.43E-05	3.08	7.01E-04	2.83	4.05E-07	3.62
5	2.19E-06	3.97	5.45E-05	3.58	2.32E-07	4.44
6	9.01E-07	6.14	5.06E-05	5.95	1.59E-07	6.87
7	7.20E-07	13.76	7.33E-05	12.52	1.18E-07	13.92
8	5.26E-07	38.07	1.11E-04	35.97	1.24E-07	37.51
9	3.93E-07	132.01	1.77E-04	130.35	1.75E-07	124.93

3 Unified wavelet algorithm for nonhomogeneous nonlinear PDE

3.1 Homotopy-based decoupled linearization

To detailed illustrate the wavelet scheme, an inhomogeneous boundary value problem in rectangular domain Ω with length L_x and width L_y is studied governed by a nonlinear partial differential equation employed as

$$\hat{\mathcal{N}}[u(X,Y)] = \psi(X,Y), \quad (X,Y) \in \Omega = [0,L_x] \times [0,L_y], \tag{3.1}$$

which can be nondimensionalized in regularization by $(x,y) = (X,Y)/L_x$ into

$$\hat{\mathcal{N}}[u(x,y)] = \mathcal{L}[u] + \mathcal{N}[u] = \psi(x,y), \quad (x,y) \in \bar{\Omega} = [0,1] \times [0,\lambda], \tag{3.2}$$

where $\hat{\mathcal{N}}$ is the nonlinear differential operator with \mathcal{L}, \mathcal{N} referring the linear and nonlinear parts, $\lambda = L_y/L_x$ is the aspect ratio of domain.

The associated generalized nonhomogeneous Cauchy boundary is

$$u|_{x=0} = B_L^d, \quad \left. \frac{\partial^{\alpha_x} u}{\partial x^{\alpha_x}} \right|_{x=0} = B_L^n, \quad u|_{x=1} = B_R^d, \quad \left. \frac{\partial^{\beta_x} u}{\partial x^{\beta_x}} \right|_{x=1} = B_R^n, \tag{3.3a}$$

$$u|_{y=0} = B_D^d, \quad \left. \frac{\partial^{\alpha_y} u}{\partial y^{\alpha_y}} \right|_{y=0} = B_D^n, \quad u|_{y=\lambda} = B_U^d, \quad \left. \frac{\partial^{\beta_y} u}{\partial y^{\beta_y}} \right|_{y=\lambda} = B_U^n, \tag{3.3b}$$

where B_i^d, B_i^n are the boundary values and derivatives of u with subscripts $i = L,R,D,U$ referring the left ($x=0$), right ($x=1$), down ($y=0$), up ($y=\lambda$) sides, $\alpha_x, \beta_x, \alpha_y, \beta_y$ are the boundary differential orders, $\psi(x,y)$ is a dual function.

If Neumann part of Eq. (3.3) is replaced by the Robin-type denoted as

$$\frac{\partial^{\alpha_x} u}{\partial x^{\alpha_x}} + k_L u = \bar{B}_L^n(y) \quad \text{on } x=0, \quad \frac{\partial^{\beta_x} u}{\partial x^{\beta_x}} + k_R u = \bar{B}_R^n(y) \quad \text{on } x=1, \tag{3.4a}$$

$$\frac{\partial^{\alpha_y} u}{\partial y^{\alpha_y}} + k_D u = \bar{B}_D^n(x) \quad \text{on } y=0, \quad \frac{\partial^{\beta_y} u}{\partial y^{\beta_y}} + k_U u = \bar{B}_U^n(x) \quad \text{on } y=\lambda, \tag{3.4b}$$

where k_i are the coefficients of source terms. With the substitution of $B_i^n = \bar{B}_i^n - k_i B_i^d$, Eq. (3.4) can be equivalently degraded into Eq. (3.3).

A transformation between a trial solution $u_0(x,y)$ with exact one $u(x,y)$ is constructed by the zeroth-order homotopy deformed equation as

$$(1-p)\hat{\mathcal{L}}[\Phi(x,y;p) - u_0(x,y)] = pc_0 \{ \hat{\mathcal{N}}[\Phi(x,y;p)] - \psi(x,y) \}, \tag{3.5}$$

where $p \in [0,1]$ denotes an embedding parameter, c_0 is the convergence-control parameter, $\hat{\mathcal{L}}$ is the auxiliary linear operator, respectively. As p evolves from 0 to 1, $\Phi(x,y;p)$ varies from the initial guess to the exact one with

$$p=0, \quad \Phi(x,y;0) = u_0(x,y), \quad p=1, \quad \Phi(x,y;1) = u(x,y). \tag{3.6}$$

Here $\Phi(x,y;p)$ can be expanded in Taylor series with respect to p as

$$\begin{aligned} \Phi(x,y;p) &= \phi(x,y;0) + \sum_{m=1}^{+\infty} \frac{1}{m!} \left. \frac{\partial^m \Phi(x,y;p)}{\partial p^m} \right|_{p=0} p^m \\ &= u_0(x,y) + \sum_{m=1}^{+\infty} u_m(x,y) p^m, \end{aligned} \tag{3.7}$$

where deformation derivative is

$$u_m(x,y) = \frac{1}{m!} \left. \frac{\partial^m \Phi(x,y;p)}{\partial p^m} \right|_{p=0}.$$

Differentiating Eq. (3.5) M times with respect to p , we obtain the M th-order deformation equations ($M \geq 1$) as

$$\hat{\mathcal{L}}[u_M - \chi_M u_{M-1}] = c_0 \{ \mathcal{L}[u_{M-1}] + \mathcal{R}_M - (1 - \chi_M) \psi \}, \tag{3.8}$$

subjected to

$$u_M = (1 - \chi_{M+1}) B_L^d(y), \quad \frac{\partial^{\alpha_x} u_M}{\partial x^{\alpha_x}} = (1 - \chi_{M+1}) B_L^n(y) \quad \text{on } x=0, \tag{3.9a}$$

$$u_M = (1 - \chi_{M+1}) B_R^d(y), \quad \frac{\partial^{\beta_x} u_M}{\partial x^{\beta_x}} = (1 - \chi_{M+1}) B_R^n(y) \quad \text{on } x=1, \tag{3.9b}$$

$$u_M = (1 - \chi_{M+1}) B_D^d(x), \quad \frac{\partial^{\alpha_y} u_M}{\partial y^{\alpha_y}} = (1 - \chi_{M+1}) B_D^n(x) \quad \text{on } y=0, \tag{3.9c}$$

$$u_M = (1 - \chi_{M+1}) B_U^d(x), \quad \frac{\partial^{\beta_y} u_M}{\partial y^{\beta_y}} = (1 - \chi_{M+1}) B_U^n(x) \quad \text{on } y=\lambda, \tag{3.9d}$$

where

$$\mathcal{R}_M = \frac{1}{(M-1)!} \frac{\partial^{M-1}}{\partial p^{M-1}} \left\{ \mathcal{N} \left[\sum_{i=0}^{M-1} u_i(x,y) p^i \right] \right\}, \quad \chi_M = \begin{cases} 0, & M \leq 1, \\ 1, & M > 1. \end{cases} \tag{3.10}$$

If the auxiliary linear operator $\hat{\mathcal{L}}$, the initial guess $u_0(x,y)$, as well as the convergence-control parameter c_0 are properly chosen to ensure the series converge at $p=1$, homotopy-series solution in M_t th truncation for $i \in [0, M_t - 1]$ are in the form of

$$U_{M_t}(x,y) = u_0(x,y) + \sum_{i=1}^{M_t-1} u_i(x,y). \tag{3.11}$$

3.2 Wavelet approximation in two-dimensional domain

To avoid complex wavelet connection coefficients [58], nonlinear item \mathcal{R}_M and ψ can be seen as a dual function generally approximated by

$$F(x,y) \approx \mathbf{P}^j[F] = \sum_{k=0}^{2^j} \sum_{l=0}^{\lambda 2^j} F\left(\frac{k}{2^j}, \frac{l}{2^j}\right) \varphi_{j,k}(x) \varphi_{j,l}(y), \quad F = \mathcal{R}_M, \psi. \quad (3.12)$$

The Coiflet-type wavelet expansion of homotopy solution $u_M(x,y)$ at each order and its derivatives with respect to Eq. (2.49) is

$$\frac{\partial^{s+t} u_M}{\partial x^s \partial y^t} \approx \sum_{k'=1}^{2^j-1} \sum_{l'=1}^{2^j-1} u_M\left(\frac{k'}{2^j}, \frac{l'}{2^j}\right) h_{j,k'}^{(s)}(x) h_{j,l'}^{(t)}(y) + (1 - \chi_{M+1})(\mathbf{B}_d^u + \mathbf{B}_n^u), \quad (3.13)$$

where \mathbf{B}_d^u is formulated by the boundary values (Dirichlet-type) and \mathbf{B}_n^u is decided by the boundary derivatives (Neumann-type) presented as

$$\begin{aligned} \mathbf{B}_d^u = & \sum_{l=0}^{\lambda 2^j} B_L^d \left(\frac{l}{2^j}\right) h_{j,0}^{(s)}(x) h_{j,l}^{(t)}(y) + B_R^d \left(\frac{l}{2^j}\right) h_{j,2^j}^{(s)}(x) h_{j,l}^{(t)}(y) \\ & + \sum_{k=0}^{2^j} B_D^d \left(\frac{k}{2^j}\right) h_{j,k}^{(s)}(x) h_{j,0}^{(t)}(y) + B_U^d \left(\frac{k}{2^j}\right) h_{j,k}^{(s)}(x) h_{j,2^j}^{(t)}(y), \end{aligned} \quad (3.14a)$$

$$\begin{aligned} \mathbf{B}_n^u = & \sum_{l=0}^{\lambda 2^j} h_{j,l}^{(t)}(y) \left[B_L^n \left(\frac{l}{2^j}\right) \omega_{j,\alpha_x}^{0,(s)}(x) + B_R^n \left(\frac{l}{2^j}\right) \omega_{j,\beta_x}^{1,(s)}(x) \right] \\ & + \sum_{k=0}^{2^j} h_{j,k}^{(s)}(x) \left[B_D^n \left(\frac{k}{2^j}\right) \omega_{j,\alpha_y}^{0,(t)}(y) + B_U^n \left(\frac{k}{2^j}\right) \omega_{j,\beta_y}^{\lambda,(t)}(y) \right], \end{aligned} \quad (3.14b)$$

and the wavelet basis with respect to Eq. (3.3) is selected as

$$h_{j,k}(x) = \varphi_{j,k}^{[0,1]} \Big|_{T_{0,k} \rightarrow T_{0,k}^N, T_{1,k} \rightarrow T_{1,k}^N}, \quad h_{j,l}(y) = \varphi_{j,l}^{[0,\lambda]} \Big|_{T_{0,l} \rightarrow T_{0,l}^N, T_{\lambda,l} \rightarrow T_{\lambda,l}^N}, \quad (3.15a)$$

$$T_{0,k}^N(x) = \sum_{i=0}^{I_{tp}} \frac{p_{0,i,k}}{i!} x^i (1 - \delta_{i,\alpha_x}), \quad T_{1,k}^N(x) = \sum_{i=0}^{I_{tp}} \frac{p_{1,i,k}}{i!} (x-1)^i (1 - \delta_{i,\beta_x}), \quad (3.15b)$$

$$T_{0,l}^N(y) = \sum_{i=0}^{I_{tp}} \frac{p_{0,i,l}}{i!} x^i (1 - \delta_{i,\alpha_y}), \quad T_{\lambda,l}^N(y) = \sum_{i=0}^{I_{tp}} \frac{p_{\lambda,i,l}}{i!} (y-\lambda)^i (1 - \delta_{i,\beta_y}), \quad (3.15c)$$

where s, t are the differential orders with admissible condition $0 \leq s+t \leq \mathbf{N}$.

Specially, for the generalized Robin-type boundary in Eq. (3.4), the wavelet basis in Eq. (3.15) will be substituted by

$$h_{j,k}(x) = \varphi_{j,k}^{[0,1]} \Big|_{T_{0,k} \rightarrow T_{0,k}^B(x), T_{1,k} \rightarrow T_{1,k}^B}, \quad h_{j,l}(y) = \varphi_{j,l}^{[0,\lambda]} \Big|_{T_{0,l} \rightarrow T_{0,l}^B, T_{\lambda,l} \rightarrow T_{\lambda,l}^B}, \quad (3.16)$$

where

$$T_{0,k}^B(x) = \sum_{i=0}^{I_{tp}} \frac{p_{0,i,k}}{i!} x^i (1 - \delta_{i,\alpha_x}) - k_L \delta_{0,k} \frac{x^{\alpha_x}}{\alpha_x!}, \tag{3.17a}$$

$$T_{1,k}^B(x) = \sum_{i=0}^{I_{tp}} \frac{p_{1,i,k}}{i!} (x-1)^i (1 - \delta_{i,\beta_x}) - k_R \delta_{0,k} \frac{(x-1)^{\beta_x}}{\beta_x!}, \tag{3.17b}$$

$$T_{0,l}^B(y) = \sum_{i=0}^{I_{tp}} \frac{p_{0,i,l}}{i!} x^i (1 - \delta_{i,\alpha_y}) - k_D \delta_{0,k} \frac{y^{\alpha_y}}{\alpha_y!}, \tag{3.17c}$$

$$T_{\lambda,l}^B(y) = \sum_{i=0}^{I_{tp}} \frac{p_{\lambda,i,l}}{i!} (y-\lambda)^i (1 - \delta_{i,\beta_y}) - k_U \delta_{0,k} \frac{(y-\lambda)^{\beta_y}}{\beta_y!}. \tag{3.17d}$$

3.3 Algebra iterative equation formulation

In view of Eq. (2.25), linear operator \mathcal{L} acting on $u(x,y)$ can be transformed into Coiflet-type wavelets as

$$\mathcal{L}[u(x,y)] \approx \mathcal{L}[\mathbf{P}^j u(x,y)] = \sum_k \sum_l u \left(\frac{k}{2^j}, \frac{l}{2^j} \right) \mathcal{L}[\varphi_{j,k}(x) \varphi_{j,l}(y)]. \tag{3.18}$$

Substituting Eq. (3.13) into Eq. (3.8) with respect to Eq. (3.18) and applying Galerkin method by multiplying $h_{j,m'}(x)h_{j,m''}(y)$ at both sides, we integrate on domain $\bar{\Omega}$ to formulate the iterating algebra equation as

$$\begin{aligned} & \tilde{\mathbf{A}}_u (\hat{\mathbf{U}}'_M - \chi_M \hat{\mathbf{U}}'_{M-1}) \\ & = c_0 \left\{ \tilde{\mathbf{B}}_u \hat{\mathbf{U}}'_{M-1} + \tilde{\mathbf{C}}_u \hat{\mathbf{R}}_M + (1 - \chi_{M+1}) (\hat{\mathbf{B}}^u - \tilde{\mathbf{C}}_u \hat{\mathbf{Q}}) \right\}, \end{aligned} \tag{3.19}$$

where the straight vectors of u_M, \mathcal{R}_M, ψ are formulated as

$$\hat{\mathbf{U}}'_M = \left\{ u_{q'} = u_M \left(\frac{k'}{2^{j'}}, \frac{l'}{2^j} \right) \right\}, \tag{3.20a}$$

$$\hat{\mathbf{R}}_M = \left\{ r_q = \mathcal{R} \left(\frac{k}{2^j}, \frac{l}{2^j} \right) \right\}, \tag{3.20b}$$

$$\hat{\mathbf{Q}} = \left\{ r_q = \psi \left(\frac{k}{2^j}, \frac{l}{2^j} \right) \right\}, \tag{3.20c}$$

$$k' = 1 \sim 2^j - 1, \quad l' = 1 \sim 2^j \lambda - 1, \quad k = 0 \sim 2^j, \quad l = 0 \sim 2^j \lambda. \tag{3.20d}$$

Iterative matrices $\tilde{\mathbf{A}}_u$ and $\tilde{\mathbf{B}}_u$ composed by wavelet connection coefficients corresponding to the auxiliary linear operator $\hat{\mathcal{L}}$ and the transformation of operators of linear part in

Eq. (3.1) are

$$\tilde{\mathbf{A}}_u^T = \left\{ \gamma_{q',o'} = \int_0^1 \int_0^\lambda \hat{\mathcal{L}}[h_{j,k'}(x)h_{j,l'}(y)]h_{j,n'}(x)h_{j,m'}(y)dx dy \right\}, \tag{3.21a}$$

$$\tilde{\mathbf{B}}_u^T = \left\{ \gamma_{q',o'} = \int_0^1 \int_0^\lambda \mathcal{L}[h_{j,k'}(x)h_{j,l'}(y)]h_{j,n'}(x)h_{j,m'}(y)dx dy \right\}, \tag{3.21b}$$

where

$$q'(k',l') = (2^j\lambda - 1)(k' - 1) + l', \quad o'(n',m') = (2^j\lambda - 1)(n' - 1) + m'. \tag{3.22}$$

The matrix $\tilde{\mathbf{C}}_u$ indicating the transformation of nonlinear item in Eq. (3.1) by Galerkin method is demonstrated as

$$\tilde{\mathbf{C}}_u^T = \left\{ \gamma_{q,o'} = \int_0^1 \varphi_{j,k}(x)h_{j,n'}(x)dx \cdot \int_0^\lambda \varphi_{j,l}(y)h_{j,m'}(y)dy \right\}, \tag{3.23}$$

in which $q(k,l) = 2^j\lambda k + l + 1$ and the crossing connection coefficients by $h_{j,k}$ with original $\varphi_{j,k}$ is

$$\bar{\Gamma}_{k,l}^{j,n,1} = \left\{ \gamma_{k,l} = \int_a^b \frac{d^n \varphi_{j,k}(x)}{dx^n} h_{j,l}(x)dx \right\}, \tag{3.24a}$$

$$\bar{\Gamma}_{k,l}^{j,n,2} = \left\{ \gamma_{k,l} = \int_a^b \frac{d^n h_{j,k}(x)}{dx^n} \varphi_{j,l}(x)dx \right\}. \tag{3.24b}$$

It should be noted that matrices $\tilde{\mathbf{A}}_u, \tilde{\mathbf{B}}_u, \tilde{\mathbf{C}}_u$ are not need to be updated in iterating process and irreverent to the unsolved problems.

The linear part of Eq. (3.1) is generally formulated expressed as

$$\begin{aligned} \mathcal{L}[f] &= \left\{ C_{mn} \frac{\partial^{m+n}}{\partial x^m \partial y^n} + \dots + C_{11} \frac{\partial^2}{\partial x \partial y} + C_{10} \frac{\partial}{\partial x} + C_{01} \frac{\partial}{\partial y} + C_{00} \right\} f \\ &= \sum_{s=0}^m \sum_{t=0}^n C_{st} \frac{\partial^{s+t} f}{\partial x^s \partial y^t}, \quad 0 \leq s \leq m, \quad 0 \leq t \leq n, \end{aligned} \tag{3.25}$$

where C_{st} are the constant coefficients.

By substituting Eq. (3.25) into Eqs. (3.21b), (3.23), $\tilde{\mathbf{B}}_u, \tilde{\mathbf{C}}_u$ can be further expressed by tensor products in terms of Eq. (2.59) as

$$\tilde{\mathbf{B}}_u^T = \sum_{s=0}^m \sum_{t=0}^n C_{st} \tilde{\Gamma}_{k',n'}^{j,s} \otimes \tilde{\Gamma}_{l',m'}^{j,t}, \quad \tilde{\mathbf{C}}_u^T = \bar{\Gamma}_{k,n'}^{j,0,1} \otimes \bar{\Gamma}_{l,m'}^{j,0,1}, \tag{3.26}$$

where \otimes denotes the Kronecker product operator.

Since the wavelet approximation in Eq. (3.13) is largely influenced by nonhomogeneous boundaries in Eqs. (3.3), (3.4) generated iterative correction $\hat{\mathbf{B}}^u$ as

$$\hat{\mathbf{B}}^u = \hat{\mathbf{B}}_d^u + \hat{\mathbf{B}}_n^u, \quad \hat{\mathbf{B}}_d^u = \sum_i \tilde{\mathbf{E}}_i^d \hat{\mathbf{P}}_i^d, \quad \hat{\mathbf{B}}_n^u = \sum_i \tilde{\mathbf{E}}_i^n \hat{\mathbf{P}}_i^n, \quad i = L, R, D, U, \tag{3.27}$$

where iterating matrices and straight vectors are

$$(\tilde{\mathbf{E}}_L^d)^T = \sum_{s=0}^m \sum_{t=0}^n C_{st} \tilde{\mathbf{\Gamma}}_{0,n'}^{j,s} \otimes \tilde{\mathbf{\Gamma}}_{l,m'}^{j,t}, \quad (\tilde{\mathbf{E}}_R^d)^T = \sum_{s=0}^m \sum_{t=0}^n C_{st} \tilde{\mathbf{\Gamma}}_{2^j,n'}^{j,s} \otimes \tilde{\mathbf{\Gamma}}_{l,m'}^{j,t}, \quad (3.28a)$$

$$(\tilde{\mathbf{E}}_D^d)^T = \sum_{s=0}^m \sum_{t=0}^n C_{st} \tilde{\mathbf{\Gamma}}_{k,n'}^{j,s} \otimes \tilde{\mathbf{\Gamma}}_{0,m'}^{j,t}, \quad (\tilde{\mathbf{E}}_U^d)^T = \sum_{s=0}^m \sum_{t=0}^n C_{st} \tilde{\mathbf{\Gamma}}_{k,n'}^{j,s} \otimes \tilde{\mathbf{\Gamma}}_{2^j\lambda,m'}^{j,t}, \quad (3.28b)$$

$$(\tilde{\mathbf{E}}_L^n)^T = \sum_{s=0}^m \sum_{t=0}^n C_{st} \hat{\mathbf{\Gamma}}_{L,n'}^{j,s} \otimes \tilde{\mathbf{\Gamma}}_{l,m'}^{j,t}, \quad (\tilde{\mathbf{E}}_R^n)^T = \sum_{s=0}^m \sum_{t=0}^n C_{st} \hat{\mathbf{\Gamma}}_{R,n'}^{j,s} \otimes \tilde{\mathbf{\Gamma}}_{l,m'}^{j,t}, \quad (3.28c)$$

$$(\tilde{\mathbf{E}}_D^n)^T = \sum_{s=0}^m \sum_{t=0}^n C_{st} \tilde{\mathbf{\Gamma}}_{k,n'}^{j,s} \otimes \hat{\mathbf{\Gamma}}_{L,m'}^{j,t}, \quad (\tilde{\mathbf{E}}_U^n)^T = \sum_{s=0}^m \sum_{t=0}^n C_{st} \tilde{\mathbf{\Gamma}}_{k,n'}^{j,s} \otimes \hat{\mathbf{\Gamma}}_{R,m'}^{j,t}, \quad (3.28d)$$

and

$$\hat{\mathbf{P}}_i^d = \left\{ f_k = B_i^d \left(\frac{k}{2^j} \right) \right\}, \quad \hat{\mathbf{P}}_i^n = \left\{ f_k = B_i^n \left(\frac{k}{2^j} \right) \right\}, \quad i = D, U, \quad (3.29a)$$

$$\hat{\mathbf{P}}_i^d = \left\{ f_l = B_i^d \left(\frac{l}{2^j} \right) \right\}, \quad \hat{\mathbf{P}}_i^n = \left\{ f_l = B_i^n \left(\frac{l}{2^j} \right) \right\}, \quad i = L, R. \quad (3.29b)$$

3.4 Nonlinear item approximation

Since the numerical approximation of nonlinear item in Eq. (3.8) plays a prominent role in iterative process, it can be further seen as a complicated dual coupling function composed of the vectors of $u_i(x,y)$ and its partial derivatives $\frac{\partial^{s+t} u_i(x,y)}{\partial x^s \partial y^t}$ along with their products expressed as

$$\mathcal{R}_M(x,y) = f \left[\bar{\mathbf{u}}, \frac{\partial^{s+t} \bar{\mathbf{u}}}{\partial x^s \partial y^t}, \sum_{i+k=M-1} u_i \cdot \frac{\partial^{s+t} u_k}{\partial x^s \partial y^t} \right], \quad (3.30)$$

where

$$\frac{\partial^{s+t} \bar{\mathbf{u}}}{\partial x^s \partial y^t} = \left\{ \frac{\partial^{s+t} u_0}{\partial x^s \partial y^t}, \frac{\partial^{s+t} u_1}{\partial x^s \partial y^t}, \dots, \frac{\partial^{s+t} u_{M-1}}{\partial x^s \partial y^t} \right\}, \quad (3.31a)$$

$$\bar{\mathbf{u}} = \{u_0, u_1, \dots, u_{M-1}\}, \quad 0 \leq s \leq m-1, \quad 0 \leq t \leq n-1. \quad (3.31b)$$

To solve the M th iterative Eq. (3.19), the straight vector of $\bar{\mathbf{U}}_M$ has been calculated in low-order in matrix form of Eq. (3.31b) as

$$\bar{\mathbf{U}}_M = \{ \hat{\mathbf{U}}_0, \hat{\mathbf{U}}_1, \dots, \hat{\mathbf{U}}_{M-1} \}, \quad \hat{\mathbf{U}}_i = \left\{ u_q = u_i \left(\frac{k}{2^j}, \frac{l}{2^j} \right) \right\}, \quad (3.32)$$

in which $\hat{\mathbf{U}}_0$ is formulated by dyadic values of initial guess $u_0(x,y)$.

To approximate the derivatives in Eq. (3.31a) on the basis of dyadic values of homotopy solutions in Eq. (3.31b), the values at dyadic points of Eq. (3.13) is considered as

$$\hat{\mathbf{U}}_{s,t}^{M,j} = \left(\hat{\mathbf{H}}_s^j \otimes \hat{\mathbf{H}}_t^j \right)^T \hat{\mathbf{U}}_{M+1} + (1 - \chi_{M+1}) \Delta \hat{\mathbf{U}}_{s,t}^j, \quad (3.33)$$

where $\Delta \hat{\mathbf{U}}_{s,t}^j$ is generated by derivatives of nonhomogeneous boundary as

$$\Delta \hat{\mathbf{U}}_{s,t}^j = (\hat{\Phi}_{s,L}^j \otimes \hat{\mathbf{P}}_L^n + \hat{\Phi}_{s,R}^j \otimes \hat{\mathbf{P}}_R^n) \hat{\mathbf{H}}_t^j + (\hat{\mathbf{H}}_s^j)^T (\hat{\mathbf{P}}_D^n \otimes \hat{\Phi}_{t,D}^j + \hat{\mathbf{P}}_U^n \otimes \hat{\Phi}_{t,U}^j), \tag{3.34}$$

along with the derivative vectors of modified Coiflets and boundary Coiflets are

$$\hat{\mathbf{H}}_s^j = \left\{ f_k = h_{j,k}^{(s)} \left(\frac{k}{2^j} \right) \right\}, \quad \hat{\mathbf{H}}_t^j = \left\{ f_l = h_{j,l}^{(t)} \left(\frac{l}{2^j} \right) \right\}, \tag{3.35a}$$

$$\hat{\Phi}_{s,L}^j = \left\{ f_k = \omega_{j,\alpha_x}^{0,(s)} \left(\frac{k}{2^j} \right) \right\}, \quad \hat{\Phi}_{s,R}^j = \left\{ f_k = \omega_{j,\beta_x}^{1,(s)} \left(\frac{k}{2^j} \right) \right\}, \tag{3.35b}$$

$$\hat{\Phi}_{t,D}^j = \left\{ f_l = \omega_{j,\alpha_y}^{0,(t)} \left(\frac{l}{2^j} \right) \right\}, \quad \hat{\Phi}_{t,U}^j = \left\{ f_l = \omega_{j,\beta_y}^{\lambda,(t)} \left(\frac{l}{2^j} \right) \right\}. \tag{3.35c}$$

Then, matrices of dyadic values with respect to the Eq. (3.31a) are further implemented by

$$\vec{\mathbf{U}}_{s,t}^{M,j} = \left\{ \hat{\mathbf{U}}_{s,t}^{0,j}, \hat{\mathbf{U}}_{s,t}^{1,j}, \dots, \hat{\mathbf{U}}_{s,t}^{M-1,j} \right\}. \tag{3.36}$$

Combining the Eqs. (3.30), (3.32), (3.36) within the framework of wavelet method, non-linear item is finally approximated by

$$\hat{\mathbf{R}}_M = f \left[\vec{\mathbf{U}}_M, \vec{\mathbf{U}}_{s,t}^{M,j}, \sum_{i+k=M-1} \hat{\mathbf{U}}_i \odot \hat{\mathbf{U}}_{s,t}^{k,j} \right], \tag{3.37}$$

where \odot denotes the operator of Schur product.

Finally, in view of Eqs. (3.32), (3.34), the M_t th truncated solution $U_{M_t}(x,y)$ in Eq. (3.11) is numerically reconstituted at dyadic points form as

$$\hat{\mathbf{U}}_{M_t} = \hat{\mathbf{U}}_0 + \sum_{i=1}^{M_t-1} \hat{\mathbf{U}}_i + \Delta \hat{\mathbf{U}}_{0,0}^j, \quad \hat{\mathbf{U}}_{M_t} = \left\{ f_q = U_{M_t} \left(\frac{k}{2^j}, \frac{l}{2^j} \right) \right\}. \tag{3.38}$$

Compared to the other homotopy-based methods, the typical characteristic of wavelet-based approach takes full advantage of high-precision approximating property of Coiflet in nonhomogeneous nonlinear boundary value problems on arbitrary rectangular domain, which specifically adopts Galerkin method in solving higher-order deformed Eq. (3.8).

3.5 Computational complexity analysis

To further study the computational process, iterative Eq. (3.19) is rewritten as

$$\hat{\mathbf{U}}_M = (c_0 + \chi_M) \tilde{\mathbf{B}}_u \hat{\mathbf{U}}_{M-1} + c_0 \tilde{\mathbf{C}}_u \tilde{\mathbf{R}}_M + c_0 (1 - \chi_{M+1}) \hat{\mathbf{P}}, \tag{3.39}$$

where

$$\tilde{\mathbf{B}}_u = \tilde{\mathbf{A}}_u^{-1} \tilde{\mathbf{B}}_u, \quad \tilde{\mathbf{C}}_u = \tilde{\mathbf{A}}_u^{-1} \tilde{\mathbf{C}}_u, \quad \hat{\mathbf{P}} = \tilde{\mathbf{A}}_u^{-1} \left(\hat{\mathbf{B}}_d^u + \hat{\mathbf{B}}_n^u - \tilde{\mathbf{C}}_u \hat{\mathbf{Q}} \right), \tag{3.40}$$

which can be written at each step as

$$\hat{U}_1 = c_0 \tilde{B}_u \hat{U}_0 + c_0 \tilde{C}_u \hat{R}_1 + c_0 \hat{P}, \tag{3.41a}$$

$$\hat{U}_2 = (c_0 + 1) \tilde{B}_u \hat{U}_1 + c_0 \tilde{C}_u \hat{R}_2, \dots, \tag{3.41b}$$

$$\hat{U}_{M_t-1} = (c_0 + 1) \tilde{B}_u \hat{U}_{M_t-2} + c_0 \tilde{C}_u \hat{R}_{M_t-1}. \tag{3.41c}$$

The foremost procedure in the exhibited wavelet technique is to set up a database of highly accurate connection coefficients [58] in Eqs. (2.59), (3.24) and exchange algorithm of data layers. To delve into the computational cost in solving the iterative Eq. (3.39), the construction of dense matrices $\tilde{B}_u, \tilde{C}_u, \hat{P}$ can be stored advanced in memory at different resolution level j , which should be considered in terms of a single dense matrix operator \tilde{A}_u .

Matrices formulation of $\tilde{A}_u, \tilde{B}_u, \tilde{C}_u$ stems from tensor products of connection coefficients in Eqs. (3.26), (3.28) with $\mathcal{O}(N_1^2)$ operations as

$$C_{mlt}[\tilde{A}_u] = \bar{K}_a N_1^2, \quad C_{mlt}[\tilde{B}_u] = \bar{K}_b N_1^2, \quad C_{mlt}[\tilde{C}_u] = N_1 N_2, \tag{3.42a}$$

$$C_{add}[\tilde{A}_u] = \bar{K}_a N_1^2, \quad C_{add}[\tilde{B}_u] = \bar{K}_b N_1^2, \quad C_{add}[\tilde{C}_u] = 0, \tag{3.42b}$$

$$N_1 = (2^j - 1)(2^j \lambda - 1), \quad N_2 = (2^j + 1)(2^j \lambda + 1), \tag{3.42c}$$

in which C_{mlt}, C_{add} are the operating numbers of multiplication and addition, the constant \bar{K}_a is determined by auxiliary linear operator \hat{L} , while constant $\bar{K}_b = (\mathbf{m} + 1)(\mathbf{n} + 1)$ is decided by the operator in Eq. (3.25).

Then, a solution process is implemented to obtain $(\tilde{A}_u)^{-1}$ by inverting the $\mathbb{R}^{N_1 \times N_1}$ matrix in $\mathcal{O}(N_1^3)$ multiplicative complexity, while the remaining cost of constructing \tilde{B}_u, \tilde{C}_u in Eq. (3.40) by $\mathcal{O}(N_1^3)$ matrix multiplication is

$$C_{mlt}[\tilde{B}_u] = C_{mlt}[\tilde{C}_u] = N_1^3, \quad C_{add}[\tilde{B}_u] = C_{add}[\tilde{C}_u] = N_1^2(N_1 - 1). \tag{3.43}$$

The computing complexity of correction matrix \hat{P} is studied appeared only in zeroth iterative equation, in which \hat{B}^u is composed of connection coefficients from nonhomogeneous boundaries in Eq. (3.27) as

$$C_{mlt}[\hat{B}^u] = 4N_1[2^j + 2^j \lambda + 2](\bar{K}_b + 1) \sim \mathcal{O}(N_1^{3/2}), \tag{3.44a}$$

$$C_{add}[\hat{B}^u] = 4N_1[2^j + 2^j \lambda + 2]\bar{K}_b + 4N_1 2^j(1 + \lambda) + 6N_1 \sim \mathcal{O}(N_1^{3/2}). \tag{3.44b}$$

Hence, the computing cost of \hat{P} is behaved as

$$C_{mlt}[\hat{P}] = N_2 N_1 + N_1^3 + C_{mlt}[\hat{B}^u] \sim \mathcal{O}(N_1^3), \tag{3.45a}$$

$$C_{add}[\hat{P}] = 2N_1 + (N_2 - 1)N_1 + N_1(N_1 - 1) + C_{add}[\hat{B}^u] \sim \mathcal{O}(N_1^3). \tag{3.45b}$$

The calculation of matrices $\tilde{B}_u, \tilde{C}_u, \hat{P}$ is significant part of the overall computational cost without repeatedly formulated at each iterative step.

The primary work of investigating the nonlinear term R_M is to evaluate $\hat{\mathbf{U}}_{s,t}^{M,j}$ composed by tensor products $\hat{\mathbf{H}}_s^j \otimes \hat{\mathbf{H}}_t^j$ and $\Delta \hat{\mathbf{U}}_{s,t}^j$ defined in Eq. (3.33), which can be constructed in advanced with complexity of $C_{mlt}[\hat{\mathbf{H}}_s^j \otimes \hat{\mathbf{H}}_t^j] = N_2$, $C_{add}[\Delta \hat{\mathbf{U}}_{m,n}^j] = 3N_2$ and

$$C_{mlt}[\Delta \hat{\mathbf{U}}_{m,n}^j] = N_2(2^j + 1 + 2^j \lambda + 1) \sim \mathcal{O}(N_2^{3/2}). \tag{3.46}$$

4 Bending of orthotropic plate with forced restraints

4.1 Governing equation

To apply the wavelet strategy in solving nonlinear problem with nonhomogeneous boundaries, large-deflection bending analysis of orthotropic plate with length L_x , width L_y and thickness h on nonlinear orthotropic foundation [59] with forced rotational boundary restraints is considered in Fig. 2. The origin of coordination system is located at the corner and the X, Y axes are along the orientations of plate length and width with governing equations by

$$\begin{aligned} & D_x \frac{\partial^4 W}{\partial X^4} + 2H \frac{\partial^4 W}{\partial X^2 \partial Y^2} + D_y \frac{\partial^4 W}{\partial Y^4} + K_1 W + K_2 W^3 \\ & - G_\zeta \left(\cos^2 \Theta \frac{\partial^2 W}{\partial X^2} + \sin 2\Theta \frac{\partial^2 W}{\partial X \partial Y} + \sin^2 \Theta \frac{\partial^2 W}{\partial Y^2} \right) \\ & - G_\eta \left(\sin^2 \Theta \frac{\partial^2 W}{\partial X^2} - \sin 2\Theta \frac{\partial^2 W}{\partial X \partial Y} + \cos^2 \Theta \frac{\partial^2 W}{\partial Y^2} \right) \\ & - h \left(\frac{\partial^2 W}{\partial X^2} \frac{\partial^2 \Psi}{\partial Y^2} + \frac{\partial^2 W}{\partial Y^2} \frac{\partial^2 \Psi}{\partial X^2} - 2 \frac{\partial^2 W}{\partial X \partial Y} \frac{\partial^2 \Psi}{\partial X \partial Y} \right) = Q, \end{aligned} \tag{4.1a}$$

$$\frac{1}{E_y} \frac{\partial^4 \Psi}{\partial X^4} + \left(\frac{1}{G} - 2 \frac{\nu_x}{E_x} \right) \frac{\partial^4 \Psi}{\partial X^2 \partial Y^2} + \frac{1}{E_x} \frac{\partial^4 \Psi}{\partial Y^4} + \left[\frac{\partial^2 W}{\partial X^2} \frac{\partial^2 W}{\partial Y^2} - \left(\frac{\partial^2 W}{\partial X \partial Y} \right)^2 \right] = 0, \tag{4.1b}$$

subjected to $W|_{\partial\Omega} = 0$ and

$$M_x = -D_x \left(\frac{\partial^2 W}{\partial X^2} + \nu_y \frac{\partial^2 W}{\partial Y^2} \right) = -M_L \quad \text{on } X=0, \tag{4.2a}$$

$$M_x = -D_x \left(\frac{\partial^2 W}{\partial X^2} + \nu_y \frac{\partial^2 W}{\partial Y^2} \right) = -M_R \quad \text{on } X=L_x, \tag{4.2b}$$

$$\theta_y = \frac{\partial W}{\partial Y} = \theta_D \quad \text{on } Y=0, \quad \theta_y = \frac{\partial W}{\partial Y} = \theta_U \quad \text{on } Y=L_y, \tag{4.2c}$$

where W, Ψ are the transverse displacement and Airy stress function, Q is the external load, G is the shear modulus, D_x, D_y and E_x, E_y are the flexural rigidity and the elasticity modulus in X, Y orientations, $H = \nu_y D_x + 2D_{xy} = \nu_x D_y + 2D_{xy}$ is the effectively torsional rigidity where D_{xy} is the torsional rigidity and ν_x, ν_y are the Poisson's ratios, M_L, M_R and

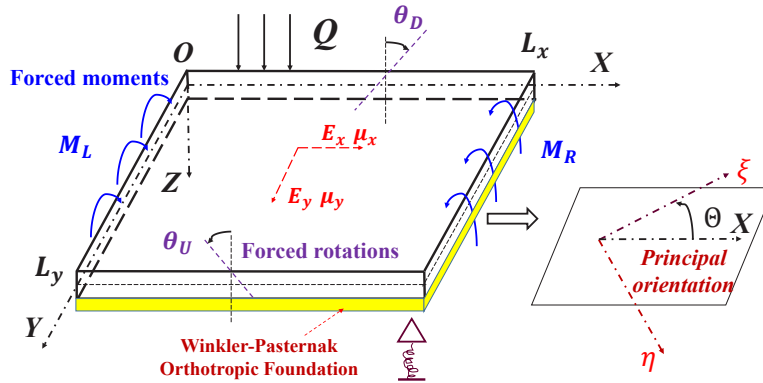


Figure 2: Schematic diagram of orthotropic plate on foundation with forced boundary rotations and moments.

θ_D, θ_U are the forced moments and rotations, K_1, K_2 are the linear and nonlinear Winkler-type foundation parameters, G_ζ, G_η are the orthotropic Pasternak-type shear foundation parameters in ζ and η principle directions respectively, the angle Θ describes the local ζ orientation of orthotropic foundation with respect to the global X-axis.

By introducing

$$x = \frac{X}{L_x}, \quad y = \frac{Y}{L_x}, \quad w = \frac{W}{h}, \quad \varphi = \frac{\Psi h}{D_x}, \quad \lambda = \frac{L_y}{L_x}, \quad (4.3a)$$

$$q = \frac{QL_x^4}{D_x h'}, \quad \bar{M}_i = \frac{M_i L_x^2}{D_x h'}, \quad \bar{\theta}_i = \frac{\theta_i L_x}{h}, \quad \varepsilon_1 = \frac{D_y}{D_x}, \quad \varepsilon_2 = \frac{H}{D_x}, \quad (4.3b)$$

$$\varepsilon_3 = \frac{E_x}{G} - 2\nu_x, \quad k_1 = \frac{K_1 L_x^4}{D_x}, \quad k_2 = \frac{K_2 h^2 L_x^4}{D_x}, \quad g_\zeta = \frac{G_\zeta L_x^2}{D_x}, \quad g_\eta = \frac{G_\eta L_x^2}{D_x}, \quad (4.3c)$$

Eqs. (4.1), (4.1b), (4.2) are nondimensionalized into $\bar{\Omega} = [0,1] \times [0,\lambda]$ as

$$\frac{\partial^4 w}{\partial x^4} + 2\varepsilon_2 \frac{\partial^4 w}{\partial x^2 \partial y^2} + \varepsilon_1 \frac{\partial^4 w}{\partial y^4} + k_1 w + k_2 w^3 - L_P[w] - \left(\frac{\partial^2 w}{\partial x^2} \frac{\partial^2 \varphi}{\partial y^2} + \frac{\partial^2 w}{\partial y^2} \frac{\partial^2 \varphi}{\partial x^2} - 2 \frac{\partial^2 w}{\partial x \partial y} \frac{\partial^2 \varphi}{\partial x \partial y} \right) = q, \quad (4.4a)$$

$$\frac{1}{\varepsilon_1} \frac{\partial^4 \varphi}{\partial x^4} + \varepsilon_3 \frac{\partial^4 \varphi}{\partial x^2 \partial y^2} + \frac{\partial^4 \varphi}{\partial y^4} + K_e \left[\frac{\partial^2 w}{\partial x^2} \frac{\partial^2 w}{\partial y^2} - \left(\frac{\partial^2 w}{\partial x \partial y} \right)^2 \right] = 0, \quad (4.4b)$$

where $K_e = 12(1 - \mu^2)$ and

$$L_P[w] = g_\zeta \left(\cos^2 \Theta \frac{\partial^2}{\partial x^2} + \sin 2\Theta \frac{\partial^2}{\partial x \partial y} + \sin^2 \Theta \frac{\partial^2}{\partial y^2} \right) + g_\eta \left(\sin^2 \Theta \frac{\partial^2}{\partial x^2} - \sin 2\Theta \frac{\partial^2}{\partial x \partial y} + \cos^2 \Theta \frac{\partial^2}{\partial y^2} \right) w, \quad (4.5)$$

associated with nonhomogeneous Cauchy boundary as $w|_{\partial\bar{\Omega}} = 0$ and

$$\left. \frac{\partial^2 w}{\partial x^2} \right|_{x=0} = \bar{M}_L, \quad \left. \frac{\partial^2 w}{\partial x^2} \right|_{x=1} = \bar{M}_R, \quad \left. \frac{\partial w}{\partial y} \right|_{y=0} = \bar{\theta}_D, \quad \left. \frac{\partial w}{\partial y} \right|_{y=\lambda} = \bar{\theta}_U, \quad (4.6)$$

where λ is the aspect ratio of orthotropic plate, q denotes the lateral load and w, φ are the deflection and Airy function in dimensionless form, \bar{M}_L, \bar{M}_R and $\bar{\theta}_U, \bar{\theta}_D$ are the dimensionless forced boundary moments and rotations, $\varepsilon_1, \varepsilon_2, \varepsilon_3$ are the orthotropic parameters, k_1, k_2 are the dimensionless linear and nonlinear Winkler parameters, g_{ξ}, g_{η} are the dimensionless Pasternak shear foundation parameters, respectively. Specially for linear bending of orthotropic plate on nonlinear Winkler-Pasternak foundation, Eq. (4.4a) will be degraded into

$$\frac{\partial^4 w}{\partial x^4} + 2\varepsilon_2 \frac{\partial^4 w}{\partial x^2 \partial y^2} + \varepsilon_1 \frac{\partial^4 w}{\partial y^4} + k_1 w + k_2 w^3 - L_P[w] = q. \quad (4.7)$$

4.2 Homotopy-based wavelet implementation

Homotopy-based transformation is constructed formulating zeroth deformed equations with respect to Eq. (3.5) as

$$\left. \begin{aligned} (1-p)\hat{\mathcal{L}}_w[\Phi(x,y;p) - w_0(x,y)] &= pc_1 \hat{\mathcal{N}}_w[\Phi(x,y;p), \Theta(x,y;p)] \\ (1-p)\hat{\mathcal{L}}_\varphi[\Theta(x,y;p) - \varphi_0(x,y)] &= pc_2 \hat{\mathcal{N}}_\varphi[\Phi(x,y;p), \Theta(x,y;p)] \end{aligned} \right\}, \quad (4.8)$$

where w_0, φ_0 are the initial guesses, c_1, c_2 are the convergence control parameters, $\hat{\mathcal{L}}_w, \hat{\mathcal{L}}_\varphi$ are the auxiliary linear operators employed as

$$\hat{\mathcal{L}}_w = \frac{\partial^4}{\partial x^4} + 2\varepsilon_2 \frac{\partial^4}{\partial x^2 \partial y^2} + \varepsilon_1 \frac{\partial^4}{\partial y^4}, \quad \hat{\mathcal{L}}_\varphi = \frac{1}{\varepsilon_1} \frac{\partial^4}{\partial x^4} + \varepsilon_3 \frac{\partial^4}{\partial x^2 \partial y^2} + \frac{\partial^4}{\partial y^4}, \quad (4.9)$$

while the nonlinear operators $\hat{\mathcal{N}}_w, \hat{\mathcal{N}}_\varphi$ are

$$\begin{aligned} \hat{\mathcal{N}}_w[\Phi, \Theta] &= \mathcal{L}_w[\Phi] + k_1 \Phi + k_2 \Phi^3 - L_P[\Phi] \\ &\quad - \left(\frac{\partial^2 \Phi}{\partial x^2} \frac{\partial^2 \Theta}{\partial y^2} + \frac{\partial^2 \Phi}{\partial y^2} \frac{\partial^2 \Theta}{\partial x^2} - 2 \frac{\partial^2 \Phi}{\partial x \partial y} \frac{\partial^2 \Theta}{\partial x \partial y} \right) - q, \end{aligned} \quad (4.10a)$$

$$\hat{\mathcal{N}}_\varphi[\Phi, \Theta] = \mathcal{L}_\varphi[\Theta] + K_e \left[\frac{\partial^2 \Phi}{\partial x^2} \frac{\partial^2 \Phi}{\partial y^2} - \left(\frac{\partial^2 \Phi}{\partial x \partial y} \right)^2 \right]. \quad (4.10b)$$

The M th decoupled equations ($M \geq 1$) with respect to Eq. (3.8) are

$$\left. \begin{aligned} \hat{\mathcal{L}}_w[w_M - \chi_M w_{M-1}] &= c_1 \{ \mathcal{L}_w[w_{M-1}] + R_M^w + (\chi_M - 1)q \} \\ \hat{\mathcal{L}}_\varphi[\varphi_M - \chi_M \varphi_{M-1}] &= c_2 \{ \mathcal{L}_\varphi[\varphi_{M-1}] + R_M^\varphi \} \end{aligned} \right\}, \quad (4.11)$$

subjected to

$$\left. \begin{aligned} w_M|_{\partial\Omega} = \varphi_M|_{\partial\Omega} = \frac{\partial^2 \varphi_M}{\partial \mathbf{n}^2} \Big|_{\partial\Omega} &= 0, \\ \frac{\partial^2 w_M}{\partial x^2} \Big|_{x=0} &= (1 - \chi_{M+1}) \overline{M}_L, \quad \frac{\partial^2 w_M}{\partial x^2} \Big|_{x=1} = (1 - \chi_{M+1}) \overline{M}_R, \\ \frac{\partial w_M}{\partial y} \Big|_{y=0} &= (1 - \chi_{M+1}) \overline{\theta}_D, \quad \frac{\partial w_M}{\partial y} \Big|_{y=\lambda} = (1 - \chi_{M+1}) \overline{\theta}_U, \end{aligned} \right\}, \quad (4.12)$$

where

$$\mathcal{L}_\varphi = \hat{\mathcal{L}}_\varphi, \quad \mathcal{L}_w = \frac{\partial^4}{\partial x^4} + 2\varepsilon_2 \frac{\partial^4}{\partial x^2 \partial y^2} + \varepsilon_1 \frac{\partial^4}{\partial y^4} + k_1 w - L_p[w], \quad (4.13a)$$

$$\begin{aligned} R_M^w &= k_2 \sum_{s=0}^{M-1} \sum_{t=0}^{M-1-s} w_s w_t w_{M-1-s-t} \\ &\quad - \sum_{t=0}^{M-1} \left(\frac{\partial^2 w_s}{\partial x^2} \frac{\partial^2 \varphi_{M-1-s}}{\partial y^2} + \frac{\partial^2 w_s}{\partial y^2} \frac{\partial^2 \varphi_{M-1-s}}{\partial x^2} - 2 \frac{\partial^2 w_s}{\partial x \partial y} \frac{\partial^2 \varphi_{M-1-s}}{\partial x \partial y} \right), \end{aligned} \quad (4.13b)$$

$$R_M^\varphi = K_e \sum_{s=0}^{M-1} \left(\frac{\partial^2 w_s}{\partial x^2} \frac{\partial^2 w_{M-1-s}}{\partial y^2} - \frac{\partial^2 w_s}{\partial x \partial y} \frac{\partial^2 w_{M-1-s}}{\partial x \partial y} \right). \quad (4.13c)$$

The Coiflets expansions of w_M , φ_M and their second-order partial derivatives in nonlinear parts \mathcal{R}_M^w , \mathcal{R}_M^φ can be further approximated by

$$\frac{\partial^{u+v} w_M}{\partial x^u \partial y^v} \approx \sum_{k=1}^{2^j-12^j\lambda-1} \sum_{l=1}^{2^j-12^j\lambda-1} w_M \left(\frac{k}{2^j}, \frac{l}{2^j} \right) h_{j,k}^{(u)}(x) h_{j,l}^{(v)}(y) + (1 - \chi_{M+1}) \mathbf{B}_n^w, \quad (4.14a)$$

$$\frac{\partial^{u+v} \varphi_M}{\partial x^u \partial y^v} \approx \sum_{k=1}^{2^j-12^j\lambda-1} \sum_{l=1}^{2^j-12^j\lambda-1} \varphi_M \left(\frac{k}{2^j}, \frac{l}{2^j} \right) h_{j,k}^{(u)}(x) h_{j,l}^{(v)}(y), \quad (u,v) = (2,0), (0,2), (1,1), \quad (4.14b)$$

where

$$h_{j,k}^w(x) = \phi_{j,k}^{[0,1]}(x) |_{p_{0,2,i} \rightarrow 0, p_{1,2,i} \rightarrow 0}, \quad h_{j,k}^w(y) = \phi_{j,k}^{[0,\lambda]}(y) |_{p_{0,1,i} \rightarrow 0, p_{1,1,i} \rightarrow 0}, \quad (4.15a)$$

$$h_{j,k}^\varphi(x) = \phi_{j,k}^{[0,1]}(x) |_{p_{0,2,i} \rightarrow 0, p_{1,2,i} \rightarrow 0}, \quad h_{j,k}^\varphi(y) = \phi_{j,k}^{[0,\lambda]}(y) |_{p_{0,2,i} \rightarrow 0, p_{\lambda,2,i} \rightarrow 0}, \quad (4.15b)$$

and

$$\begin{aligned} \mathbf{B}_n^w &= \sum_{l=0}^{\lambda 2^j} h_{j,l}^{w,(v)}(y) \left[\overline{M}_L \left(\frac{l}{2^j} \right) \omega_{j,\alpha_x}^{0,(u)}(x) + \overline{M}_R \left(\frac{l}{2^j} \right) \omega_{j,\beta_x}^{1,(u)}(x) \right] \\ &\quad + \sum_{k=0}^{2^j} h_{j,k}^{w,(u)}(x) \left[\overline{\theta}_D \left(\frac{k}{2^j} \right) \omega_{j,\alpha_y}^{0,(v)}(y) + \overline{\theta}_U \left(\frac{k}{2^j} \right) \omega_{j,\beta_y}^{\lambda,(v)}(y) \right]. \end{aligned} \quad (4.16)$$

By substituting Eqs. (4.14a), (4.14b) into Eq. (4.11) applying Eq. (3.18) to construct decoupled iterative equations, Eq. (3.30) can be specified as

$$\mathcal{R}_M^w(x,y) = f \left[\vec{w}(x,y), \frac{\partial^2 \vec{w}(x,y)}{\partial x^2}, \frac{\partial^2 \vec{w}(x,y)}{\partial y^2}, \frac{\partial^2 \vec{\varphi}(x,y)}{\partial x^2}, \frac{\partial^2 \vec{\varphi}(x,y)}{\partial y^2} \right], \tag{4.17a}$$

$$\mathcal{R}_M^\varphi(x,y) = f \left[\vec{w}(x,y), \frac{\partial^2 \vec{w}(x,y)}{\partial x^2}, \frac{\partial^2 \vec{w}(x,y)}{\partial y^2} \right]. \tag{4.17b}$$

Finally, the decoupled iterating algebra equations by wavelet Galerkin method are

$$\hat{\mathbf{W}}_M = (\chi_M + c_1 \tilde{\mathbf{A}}_w^{-1} \tilde{\mathbf{B}}_w) \hat{\mathbf{W}}_{M-1} + c_1 \tilde{\mathbf{A}}_w^{-1} \tilde{\mathbf{C}} \hat{\mathbf{R}}_{M-1}^w + (\chi_M - 1) c_1 \hat{\mathbf{P}}, \tag{4.18a}$$

$$\hat{\mathbf{\Phi}}_M = (\chi_M + c_2) \hat{\mathbf{\Phi}}_{M-1} + c_2 \tilde{\mathbf{A}}_\varphi^{-1} \tilde{\mathbf{C}} \hat{\mathbf{R}}_{M-1}^\varphi, \quad \hat{\mathbf{P}} = \tilde{\mathbf{A}}_w^{-1} (\hat{\mathbf{B}}_n^w - \tilde{\mathbf{C}} \hat{\mathbf{Q}}), \tag{4.18b}$$

where straight vectors and iterating matrices are

$$\hat{\mathbf{F}} = \left\{ f_{p'} = f \left(\frac{k'}{2^j}, \frac{l'}{2^j} \right) \right\}, \quad f = w_M, \varphi_M, \quad \mathbf{F} = \mathbf{W}_M, \mathbf{\Phi}_M,$$

$$\hat{\mathbf{F}} = \left\{ f_p = f \left(\frac{k}{2^j}, \frac{l}{2^j} \right) \right\}, \quad f = R_M^w, R_M^\varphi, q, \quad \mathbf{F} = \mathbf{R}_M^w, \mathbf{R}_M^\varphi, \mathbf{Q},$$

and

$$\tilde{\mathbf{A}}_w^T = \tilde{\Gamma}_{k',n'}^{j,4} \otimes \tilde{\Gamma}_{l',m'}^{j,0} + 2\varepsilon_2 \tilde{\Gamma}_{k',n'}^{j,2} \otimes \tilde{\Gamma}_{l',m'}^{j,2} + \varepsilon_1 \tilde{\Gamma}_{k',n'}^{j,0} \otimes \tilde{\Gamma}_{l',m'}^{j,4}, \quad \tilde{\mathbf{C}}^T = \tilde{\Gamma}_{k,n'}^{j,0,1} \otimes \tilde{\Gamma}_{l,m'}^{j,0,1}, \tag{4.19a}$$

$$\begin{aligned} \tilde{\mathbf{B}}_w^T &= \tilde{\mathbf{A}}_w^T + k_1 \tilde{\Gamma}_{k',n'}^{j,0} \otimes \tilde{\Gamma}_{l',m'}^{j,0} \\ &\quad - g_\xi \left(\cos^2 \Theta \tilde{\Gamma}_{k',n'}^{j,2} \otimes \tilde{\Gamma}_{l',m'}^{j,0} + \sin 2\Theta \tilde{\Gamma}_{k',n'}^{j,1} \otimes \tilde{\Gamma}_{l',m'}^{j,1} + \sin^2 \Theta \tilde{\Gamma}_{k',n'}^{j,0} \otimes \tilde{\Gamma}_{l',m'}^{j,2} \right) \\ &\quad - g_\eta \left(\sin^2 \Theta \tilde{\Gamma}_{k',n'}^{j,2} \otimes \tilde{\Gamma}_{l',m'}^{j,0} - \sin 2\Theta \tilde{\Gamma}_{k',n'}^{j,1} \otimes \tilde{\Gamma}_{l',m'}^{j,1} + \cos^2 \Theta \tilde{\Gamma}_{k',n'}^{j,0} \otimes \tilde{\Gamma}_{l',m'}^{j,2} \right), \end{aligned} \tag{4.19b}$$

$$\tilde{\mathbf{A}}_\varphi^T = \tilde{\mathbf{B}}_\varphi^T = 1/\varepsilon_1 \tilde{\Gamma}_{k',n'}^{j,4} \otimes \tilde{\Gamma}_{l',m'}^{j,0} + \varepsilon_3 \tilde{\Gamma}_{k',n'}^{j,2} \otimes \tilde{\Gamma}_{l',m'}^{j,2} + \tilde{\Gamma}_{k',n'}^{j,0} \otimes \tilde{\Gamma}_{l',m'}^{j,4}. \tag{4.19c}$$

The matrices for nonlinear items $\hat{\mathbf{R}}_M^w, \hat{\mathbf{R}}_M^\varphi$ are specified as

$$\begin{aligned} \hat{\mathbf{R}}_M^w &= k_2 \sum_{i=0}^{M-1} \sum_{s=0}^{M-1-i} \hat{\mathbf{W}}_{0,0}^{i,j} \odot \hat{\mathbf{W}}_{0,0}^{s,j} \odot \hat{\mathbf{W}}_{0,0}^{M-1-s-i,j} \\ &\quad - \sum_{s=0}^{M-1} \left\{ \hat{\mathbf{W}}_{2,0}^{j,s} \odot \hat{\Pi}_{0,2}^{j,t} + \hat{\mathbf{W}}_{0,2}^{j,s} \odot \hat{\Pi}_{2,0}^{j,t} - 2\hat{\mathbf{W}}_{1,1}^{j,s} \odot \hat{\Pi}_{1,1}^{j,t} \right\}, \end{aligned} \tag{4.20a}$$

$$\hat{\mathbf{R}}_M^\varphi = K_e \sum_{s=0}^{M-1} \left\{ \hat{\mathbf{W}}_{2,0}^{j,s} \odot \hat{\mathbf{W}}_{0,2}^{j,t} - \hat{\mathbf{W}}_{1,1}^{j,s} \odot \hat{\mathbf{W}}_{1,1}^{j,t} \right\}, \quad t = M-1-s. \tag{4.20b}$$

in which

$$\hat{\mathbf{W}}_{u,v}^{j,M} = (\hat{\Phi}_u^j \otimes \hat{\Phi}_v^j)^T \hat{\mathbf{W}}_M^U + (1 - \chi_{M+1}) \Delta \hat{\mathbf{W}}_{u,v}^j, \quad \hat{\Pi}_{u,v}^{j,M} = (\hat{\Phi}_u^j \otimes \hat{\Phi}_v^j)^T \hat{\Phi}_M^U, \quad (4.21a)$$

$$\hat{\mathbf{W}}_M^U = \left\{ w_p = w_M \left(\frac{k}{2^j}, \frac{l}{2^j} \right) \right\}, \quad \hat{\Phi}_M^U = \left\{ \varphi_p = \varphi_M \left(\frac{k}{2^j}, \frac{l}{2^j} \right) \right\}, \quad (4.21b)$$

$$\hat{\Phi}_u^j = \left\{ f_k = h_{j,k}^{(u)} \left(\frac{k}{2^j} \right) \right\}, \quad \hat{\Phi}_v^j = \left\{ f_l = h_{j,l}^{(v)} \left(\frac{l}{2^j} \right) \right\}. \quad (4.21c)$$

5 Results and discussion

5.1 Numerical validation

Before conducting the validation, all the calculations are implemented in a Laptop (Inter(R) Core(TM) i7-8565U CPU @1.80GHz) by Mathematica 12.3. The sufficient convergent criterion is defined by the mean square error $ErrSQ_u$ tending to zero

$$ErrSQ_u = \left[\int_0^1 \int_0^\lambda E_u^2 dx dy \right]^{\frac{1}{2}} \approx \frac{1}{N_j} \sqrt{\sum_{k=0}^{2^j} \sum_{l=0}^{2^{j\lambda}} E_u^2 \left(\frac{k}{2^j}, \frac{l}{2^j} \right)}, \quad (5.1)$$

in which

$$E_u(x,y) = |U_{M_t}(x,y) - U_e(x,y)|, \quad (x,y) \in \bar{\Omega}, \quad N_j = (2^j + 1)(2^{j\lambda} + 1), \quad (5.2)$$

where U_{M_t} , U_e are the calculated and exact solutions. Nevertheless, for most cases the analytical solutions are nonexistent. The necessary convergent condition for series is $u_{M_t}(x,y) \rightarrow \mathbf{0}$ equivalent to the residual error $ErrRes_{u_{M_t}} \rightarrow 0$ given by

$$ErrRes_u = \left[\int_0^1 \int_0^\lambda u_{M_t}^2 dx dy \right]^{\frac{1}{2}} \approx \frac{1}{N_j} \sqrt{\sum_{k=0}^{2^j} \sum_{l=0}^{2^{j\lambda}} u_{M_t}^2 \left(\frac{k}{2^j}, \frac{l}{2^j} \right)}. \quad (5.3)$$

Specially when $\bar{\theta}_U, \bar{\theta}_D, \bar{M}_L, \bar{M}_R = 0$, Eq. (4.2) will be degraded into the clamped (C) or simply supported edge (S)

$$\text{Clamped: } W = \frac{\partial W}{\partial \hat{n}} = 0, \quad \text{Simply supported: } W = \frac{\partial^2 W}{\partial \hat{n}^2} = 0, \quad (5.4)$$

where \hat{n} denotes the boundary normal direction. An orthotropic plate ($\varepsilon_1 = 2, \varepsilon_2 = 1$) in linear bending on linear Winkler-Pasternak foundation ($k_1 = g_\xi = g_\eta = 1, k_2 = 0$) with aspect ratio ($\lambda = 1 \sim 5$) is investigated loaded with forced moments on circled boundaries. The absolute error $\|E_w\|_1$ and mean square error $\|E_w\|_2$ of deflection solution are elaborated in Table 3, which reveals adding the wavelet resolution level from $j=3$ to $j=6$ is significantly conducive to improving the approaching precision exponentially from 10^{-2} to 10^{-8} , but it

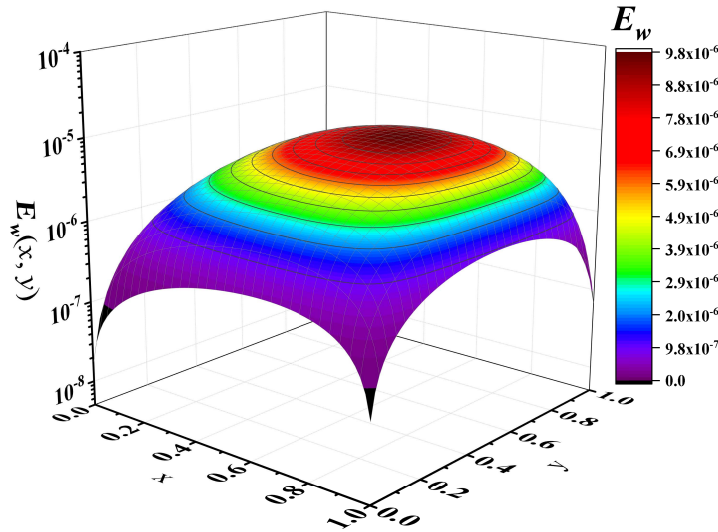


Figure 3: Absolute approaching error distribution of deflection $E_w(x,y)$ of simply supported orthotropic square plate in linear bending at wavelet resolution level $j=6$.

is not efficient by the increase of aspect ratio λ with the precision kept in the same order. In Fig. 3, the absolute error distribution at $j=6$ of deformation in orthotropic square plate is illustrated at the magnitude of 10^{-6} . The error at the circled edges is obviously suppressed with good accuracy superior to that at the plate center, which further verifies the effectiveness of foregoing wavelet strategy by improved boundary difference.

Bending of another orthotropic plate on nonlinear foundation governed by the weakly nonlinear Eq. (4.7) is studied respectively subjected to homogeneous mixed opposite edges (BC I), nonhomogeneous edges with only forced moments(BC II), only forced rotations (BC III) and both forced moments and rotations (BC IV), with the exact deflection w_e and lateral load q_e given as

$$\text{BC I: } w_e = \sin(\pi x) \left[1 - \cos\left(2\pi \frac{y}{\lambda}\right) \right], \tag{5.5a}$$

$$\text{BC II: } w_e = 64x^2(1-x)^2y^2(\lambda-y)^2, \quad \bar{M}_L = \bar{M}_R = 128y^2(\lambda-y)^2, \tag{5.5b}$$

$$\text{BC III: } w_e = 64x^3(1-x)^3y(\lambda-y), \quad \bar{\theta}_D = -\bar{\theta}_U = 64\lambda(1-x)^3x^3, \tag{5.5c}$$

$$\text{BC IV: } w_e = 64x^2(1-x)^2y(\lambda-y), \quad \bar{M}_L = \bar{M}_R = 128y(\lambda-y), \tag{5.5d}$$

$$\bar{\theta}_D = -\bar{\theta}_U = 64\lambda(1-x)^2x^2, \tag{5.5e}$$

$$q_e = \frac{\partial^4 w_e}{\partial x^4} + 2\varepsilon_2 \frac{\partial^4 w_e}{\partial x^2 \partial y^2} + \varepsilon_1 \frac{\partial^4 w_e}{\partial y^4} + k_1 w_e + k_2 w_e^3 - Lp[w_e]. \tag{5.5f}$$

As tabulated in Table 5, by selecting $c_0 = -88/100$ and $k_1, k_2, g_\xi, g_\eta = 1, \varepsilon_2 = 1, \varepsilon_1 = 2$, the approaching error of overall deflection in all cases is around $10^{-5} \sim 10^{-8}$ at $j=5$.

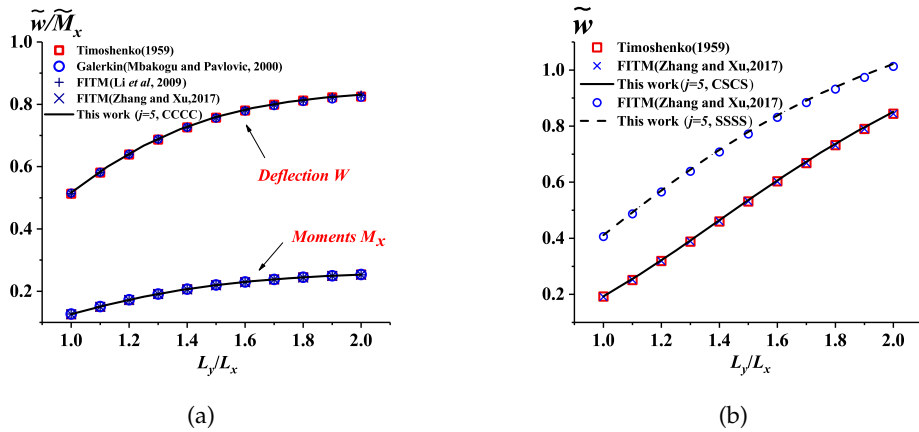


Figure 4: Comparisons of central deflection \tilde{w} and bending moment \tilde{M}_x for a uniformly loaded rectangular isotropic plate with results by Timoshenko [60], Bubnov-Galerkin method [61], Finite Integral Transform Method (FITM) [62, 63]. (a) circled clamped edge (CCCC), (b) circled simply supported (SSSS) or mixed opposite edge (CSCS).

It indicates the nonhomogeneous edges by forced boundary rotational constraints will cause the accuracy loss of transverse displacement in wavelet approximation, which is not prominently affected by the plate aspect ratio λ .

To make comparison with published results, dimensionless deflection \tilde{w} and bending moment \tilde{M}_x, \tilde{M}_y of plate under unit load are given as

$$\tilde{w} = \frac{10^3 D_x}{QL_x^4} W, \quad \tilde{M}_x = \frac{10^2 M_x}{QL_x^2}, \quad \tilde{M}_y = \frac{10^2 M_y}{QL_x^2}. \tag{5.6}$$

In Fig. 4, wavelet solutions at $j = 5$ of deflection and bending moment at the center of uniformly loaded isotropic plate ($\varepsilon_1 = \varepsilon_2 = 1$) subjected to circled clamped (CCCC), simply supported (SSSS) and mixed opposite (CSCS) edges are given in good accordance with benchmark by double trigonometric series [60], Bubnov-Galerkin method [61], Finite Integral Transform Method (FITM) [62, 63]. To conduct the quantitative analysis, Table 4 tabulates the transverse displacement and bending moments of uniformly loaded isotropic plate in different aspect ratio $\lambda = 1 \sim 5$ subjected to various boundaries, which demonstrate more significant digits in contrast with results by the Small Parameter Method (SPM) [64]. In general, the homotopy-based wavelet strategy has been validated to give highly accurate solutions for both small and large bending of orthotropic plate with forced boundary restraints performing good efficiency.

5.2 Convergence acceleration by iteration

An orthotropic rectangular plate ($\lambda = 3/2$) in small deflection subjected to homogeneous mixed edges (BC I) under load $q = 5000$ on nonlinear elastic foundation ($k_1 = g_{\zeta} = g_{\eta} = 1$,

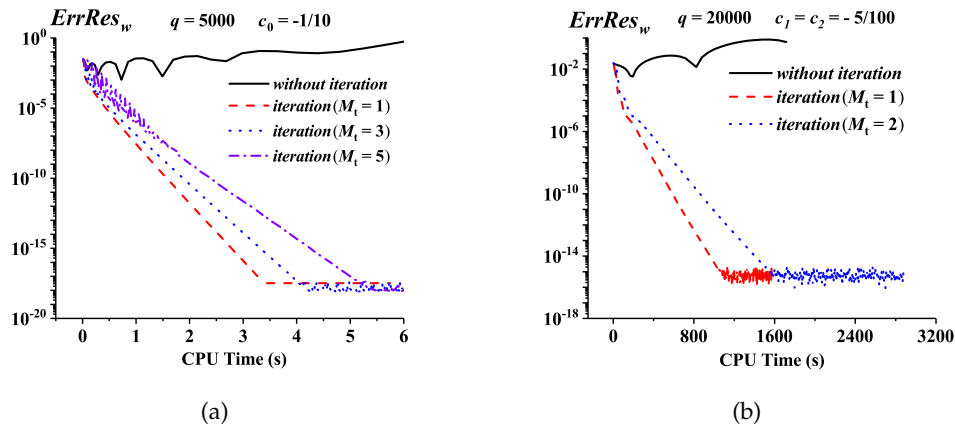


Figure 5: Residual error $ErrRes_w$ of overall deflection in (a) smally deformed orthotropic plate with homogeneous boundaries in small deflection under $q=5000$ when $\varepsilon_1=2, \varepsilon_2=1, k_1=g_{\xi}=g_{\eta}=1, k_2=50$ and (b) largely deformed clamped isotropic plate under $q=20000$ by CPU time without and with iteration ($M_t=1 \sim 5$).

$k_2 = 50$) and an isotropic plate ($\lambda = 3/2$) in extremely large deformation subjected to the circled clamped edge under load $q = 20000$ lack of foundation are investigated, which are governed by Eq. (4.7) and the coupled system of Eqs. (4.4a), (4.4b), respectively. In Fig. 5, the deflection solutions can not be guaranteed in convergence as the residual error $ErrRes_w$ diverges gradually by the homotopy-based technique (black line). By adding the truncated order M_t , the computing complexity of Eq. (4.13b) dramatically amplifies with more computing resources needed and iterative errors accumulated. In term of Eq. (4.21a), the wavelet solutions in Eq. (4.18) largely depend on the initial guess, which are also influenced by nonhomogeneous boundaries in approximation of each homotopy order resulting in difficulties of convergence.

To overcome the above obstacles, iteration is adopted by updating the initial guess \mathbf{U}_0^{iter} with the M_t th homotopy solution $\hat{\mathbf{U}}_{M_t}^{iter-1}$ as

$$\hat{\mathbf{U}}_{M_t}^{iter} = \mathbf{U}_0^{iter} + \sum_{i=1}^{M_t-1} \hat{\mathbf{U}}_i^{iter}, \quad \hat{\mathbf{U}}_0^{iter} = \hat{\mathbf{U}}_{M_t}^{iter-1}, \quad \hat{\mathbf{U}}_0^0 = \hat{\mathbf{U}}_0 + \Delta \hat{\mathbf{U}}_{0,0}^j. \quad (5.7)$$

By selecting $c_0 = -1/10$ and $c_1 = c_2 = -5/100$ updating the initial guess, the iterative process is implemented in convergence with the residual error $ErrRes_w$ decreasing to nearly 10^{-18} and 10^{-16} , respectively.

To further study the effectiveness of iterative technique by different truncated order $M_t = 1 \sim 5$, large deflection bending of orthotropic plate on weakly nonlinear foundation ($k_1 = k_2 = g_{\xi} = g_{\eta} = 1, \lambda = 3/2$) with nonhomogeneous edges (Case IV) is conducted as an example. Fig. 6 illustrates the mean square error of plate deflection varying with CPU time, which reveals the convergent rates is largely affected by the truncated order, but the accuracy of ultimate convergence is irrelevant to it. To conclude, the iterative

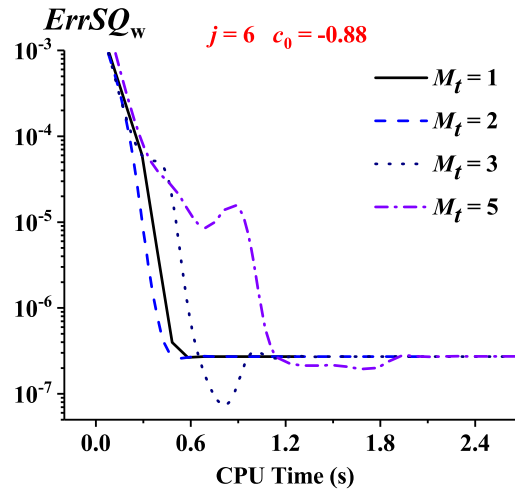


Figure 6: Mean square error $ErrSQ_w$ of deflection of orthotropic plate on weakly nonlinear foundation with nonhomogeneous boundaries (BC IV) by iteration with different truncated orders ($M_t = 1 \sim 5$) when $\varepsilon_1 = 2, \varepsilon_2 = 1, k_1 = k_2 = g_\xi = g_\eta = 1$.

technique is effective to ensure convergence in solving nonlinear bending of orthotropic plate with homogeneous or nonhomogeneous boundaries, but with no contributions to the improvement of approaching accuracy, which is only decided by wavelet resolution level.

5.3 Effect of convergence control parameter

In view of Eq. (3.5), the convergent properties of the wavelet method is largely influenced by the parameter c_0 and auxiliary linear operator $\hat{\mathcal{L}}$, while reasonable selection plays a vital role in the iterative process. The system error is defined by substituting homotopy truncated solution of Eq. (3.11) into Eq. (3.1) as

$$E_{M_t}(c_0, x, y) = \hat{\mathcal{N}}[U_{M_t}(x, y)] - \psi(x, y), \tag{5.8}$$

with the mean square error given by

$$\begin{aligned} ErrSQ_{M_t}^s &= \|E_{M_t}\|_2 = \int_0^1 \int_0^\lambda E_{M_t}^2(c_0, x, y) dx dy \\ &\approx \frac{1}{N_j} \sum_{k=0}^{2^j} \sum_{l=0}^{2^j \lambda} E_{M_t}^2 \left(c_0, \frac{k}{2^j}, \frac{l}{2^j} \right) = f(\vec{U}_{M_t}, \vec{U}_{\mathbf{m}, \mathbf{n}}^{M_t, j}, c_0). \end{aligned} \tag{5.9}$$

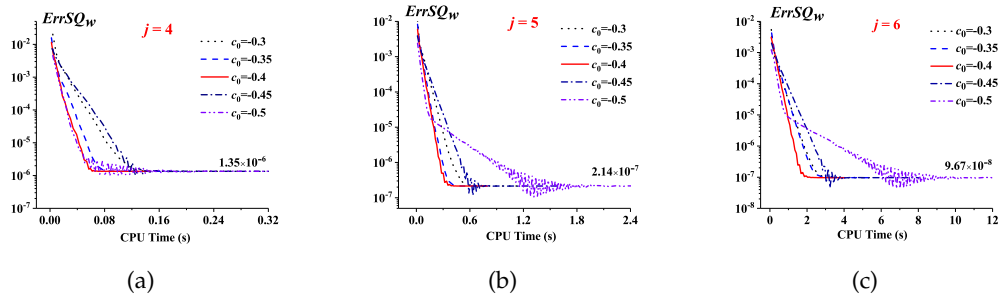


Figure 7: Convergent process of mean square error $ErrSQ_w$ of deflection of orthotropic plate on strongly nonlinear foundation ($\varepsilon_1 = 2, \varepsilon_2 = 1, k_1 = g_\xi = g_\eta = 1, k_2 = 200$) with nonhomogeneous boundaries (BC IV) by $c_0 = -3/10 \sim -5/10$. (a) $j = 4$, (b) $j = 5$, (c) $j = 6$.

Specially, if the analytical solution U_e exists, the system error $ErrSQ_{M_t}^s$ is simplified into

$$\begin{aligned}
 ErrSQ_u &= \int_0^1 \int_0^\lambda |U_e(x, y) - U_{M_t}(c_0, x, y)|^2 dx dy = f(\vec{U}_{M_t}, \vec{U}_{\mathbf{m}, \mathbf{n}}^{M_t, j}, c_0) \\
 &\approx \frac{1}{N_j} \sum_{k=0}^{2^j} \sum_{l=0}^{2^{j\lambda}} \left[U_e\left(\frac{k}{2^j}, \frac{l}{2^j}\right) - U_{M_t}\left(c_0, \frac{k}{2^j}, \frac{l}{2^j}\right) \right]^2.
 \end{aligned} \tag{5.10}$$

Bending of an orthotropic plate with inhomogeneous boundaries (Case IV) on strongly nonlinear foundation ($k_1 = g_\xi = g_\eta = 1, \lambda = 3/2, k_2 = 200$) is investigated ($M_t = 1$) in Fig. 7, while the mean square error of deflection $ErrSQ_w$ converges to $1.35 \times 10^{-6}, 2.14 \times 10^{-7}, 9.67 \times 10^{-8}$ consuming CPU time of 0.16s, 1.8s, 9s at $j = 4 \sim 6$. It reveals different selection of c_0 demonstrate various convergent rate but with duplicate accuracy at same resolution level j , while the optimal one is around $c_0 = -0.4$ with more distinct numerical oscillation in ultimate stage of convergence.

Furthermore, to study the effect of convergent parameter c_0 in a larger range showed in Fig. 8, there exist a critical value $c_{lim} = -51/100$ distinguishing the convergent range ($c_0 \geq c_{lim}$) with the divergent region ($c_0 < c_{lim}$) of the obtained deflection solutions independent of resolution level j . Based on the above analysis, c_0 can be selected firstly by rapidly trial calculation at lower wavelet resolution level to determine the critical c_{lim} and convergent range $c_0 > c_{lim}$, while the iterative computation at higher resolution level is then proceed by selecting effective c_0 to give more accurate solutions.

5.4 Effect of auxiliary linear operators

The auxiliary linear operator in the homotopy-based wavelet approach plays a vital role in the formulation of iterative matrix $\tilde{A}_w, \tilde{A}_\varphi$ in Eq. (4.18) derived from the nonlinear Eqs. (4.4a) and (4.4b). To explore the freedom in implications, a series of auxiliary linear operators are constructed by investigating the large deflection bending of circled clamped

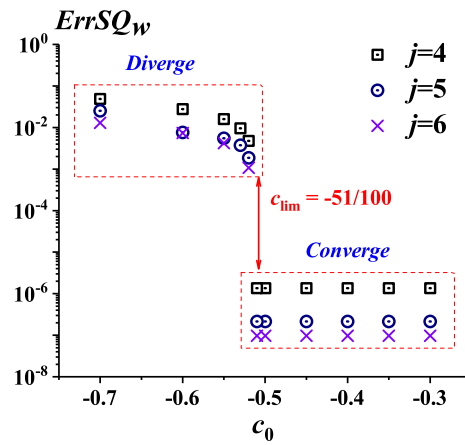


Figure 8: Convergent range of mean square error $ErrSQ_w$ of deflection of orthotropic plate on strongly nonlinear foundation ($\varepsilon_1=2, \varepsilon_2=1, k_1=g_\xi=g_\eta=1, k_2=200$) by different convergence control parameter $c_0=-7/10 \sim -3/10$ at resolution level $j=4 \sim 6$.

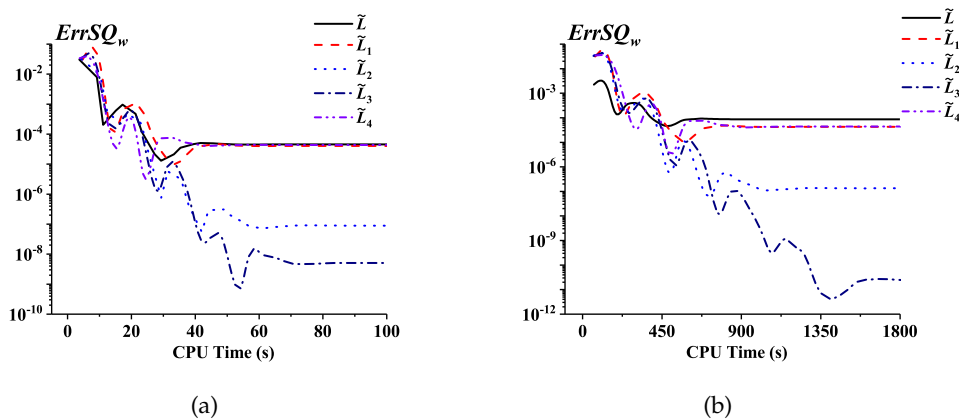


Figure 9: Convergent process of mean square error $ErrSQ$ of deflection of orthotropic plate on elastic foundation ($\varepsilon_1=2, \varepsilon_2=1, k_1=g_\xi=g_\eta=1, k_2=50$) by selecting different auxiliary linear operators $\hat{\mathcal{L}} \sim \hat{\mathcal{L}}_4$ when $c_1=c_2=-35/100$. (a) $j=5, N_j=33 \times 49$, (b) $j=6, N_j=65 \times 97$.

orthotropic plate on elastic foundation ($\lambda = 1.5, k_1 = g_\xi = g_\eta = 1, k_2 = 50$) with $\hat{\mathcal{L}}[w]$ in Eq. (4.9) substituted by

$$\hat{\mathcal{L}}_1 = \frac{\partial^4}{\partial x^4} + 2\varepsilon_2 \frac{\partial^4}{\partial x^2 \partial y^2} + \varepsilon_1 \frac{\partial^4}{\partial y^4} + k_1, \tag{5.11a}$$

$$\hat{\mathcal{L}}_2 = \frac{\partial^4}{\partial x^4} + 2\varepsilon_2 \frac{\partial^4}{\partial x^2 \partial y^2} + \varepsilon_1 \frac{\partial^4}{\partial y^4} - \left(g_\xi \frac{\partial^2}{\partial x^2} + g_\eta \frac{\partial^2}{\partial y^2} \right), \tag{5.11b}$$

$$\hat{\mathcal{L}}_3 = \frac{\partial^4}{\partial x^4} + 2\varepsilon_2 \frac{\partial^4}{\partial x^2 \partial y^2} + \varepsilon_1 \frac{\partial^4}{\partial y^4} + k_1 - \left(g_\xi \frac{\partial^2}{\partial x^2} + g_\eta \frac{\partial^2}{\partial y^2} \right), \tag{5.11c}$$

$$\hat{\mathcal{L}}_4 = \frac{\partial^4}{\partial x^4} + 2\varepsilon_2 \frac{\partial^4}{\partial x^2 \partial y^2} + \varepsilon_1 \frac{\partial^4}{\partial y^4} + k_1 - \left(g_\xi \frac{\partial^2}{\partial x^2} + g_\eta \frac{\partial^2}{\partial y^2} \right) - \left(\frac{\partial^2}{\partial x^2} + \frac{\partial^2}{\partial y^2} - \frac{\partial^2}{\partial x \partial y} \right). \tag{5.11d}$$

By selecting $c_1 = c_2 = -55/100$, the convergent process and values of mean square error of deflection $ErrSQ_w$ is illustrated in Fig. 9, which reveals different selection of auxiliary operators exhibits various convergent properties. As tabulated in Table 6, the original operator $\hat{\mathcal{L}}$ is the most concise with the fastest initial iterative speed but in the worst approaching accuracy. To refine $\hat{\mathcal{L}}$ by adding ingredients $k_1 w$ or $-\left(g_\xi \frac{\partial^2 w}{\partial x^2} + g_\eta \frac{\partial^2 w}{\partial y^2}\right)$ corresponding to the linear Winkler or Pasternak foundation, the latter reveals more effective in the improvement of precision from 10^{-4} to 10^{-7} at $j=6$, while adding both in

Table 3: Absolute error $\|E_w\|_1$ and mean square error $\|E_w\|_2$ for deflection solution of orthotropic plate ($\varepsilon_1=2, \varepsilon_2=1, k_1=g_\xi=g_\eta=1$) in linear bending with different aspect ratios $\lambda=1\sim 5$ at wavelet resolution levels $j=3\sim 6$.

L_y/L_x	$j=3, \mathbf{I}_{tp}=3$		$j=4, \mathbf{I}_{tp}=5$		$j=5, \mathbf{I}_{tp}=5$		$j=6, \mathbf{I}_{tp}=5$	
	$\ E_w\ _1$	$\ E_w\ _2$						
1	5.9E-02	4.9E-02	1.2E-05	9.7E-06	3.0E-07	2.4E-07	8.4E-08	6.7E-08
1.5	4.3E-02	4.1E-02	6.4E-06	6.1E-06	1.8E-07	1.7E-07	6.8E-08	6.7E-08
2	3.3E-02	3.6E-02	6.4E-06	7.0E-06	1.6E-07	1.8E-07	5.9E-08	6.7E-08
2.5	2.7E-02	3.3E-02	6.0E-06	7.3E-06	1.5E-07	1.8E-07	5.1E-08	6.7E-08
3	2.2E-02	3.0E-02	5.5E-06	7.4E-06	1.3E-07	1.8E-07	4.4E-08	6.7E-08
4	1.7E-02	2.7E-02	5.5E-06	7.4E-06	1.1E-07	1.7E-07	3.5E-08	6.5E-08
5	1.4E-02	2.4E-02	3.8E-06	6.6E-06	9.1E-08	1.6E-07	2.8E-08	6.4E-08

Table 4: Comparison of wavelet solution at $j=5$ for central deflection \tilde{w} and bending moments \tilde{M}_x, \tilde{M}_y of uniformly loaded isotropic plate ($\varepsilon_1 = \varepsilon_2 = 1$) with results by the Small Parameter Method (SPM) [64].

BCs	L_y/L_x	SPM [64]			This work ($j=5$)		
		\tilde{M}_x	\tilde{M}_y	\tilde{w}	\tilde{M}_x	\tilde{M}_y	\tilde{w}
SSSS	1	0.4062	0.4789	0.4789	0.406314	0.478873	0.478873
	1.5	0.7724	0.8116	0.4984	0.772465	0.811621	0.498418
	2	1.0129	1.0168	0.4635	1.01290	1.01684	0.463492
	3	1.2233	1.1886	0.4063	1.22329	1.18861	0.406259
	4	1.2819	1.2346	0.3842	1.28186	1.23458	0.384146
SCSC	1	0.1917	0.2439	0.3324	0.191739	0.243811	0.332379
	1.5	0.5326	0.5848	0.4595	0.532673	0.584768	0.459403
	2	0.8445	0.8687	0.4736	0.844520	0.868664	0.473601
SSSC	1	0.2785	0.3389	0.3918	0.278593	0.338825	0.391741
	1.5	0.6445	0.6906	0.4776	0.644555	0.690607	0.477611
	2	0.927	0.9413	0.4687	0.927048	0.941290	0.468647

Table 5: Absolute error $\|E_w\|_1$ and mean square error $\|E_w\|_2$ of deflection solution of smally deformed orthotropic plate on foundation ($\varepsilon_1=2, \varepsilon_2=1, k_1=k_2=g_\xi=g_\eta=1$) subjected to homogeneous opposite edges (BC I), nonhomogeneous edges with forced moments (BC II), forced rotations (BC III) and both forced moments and rotations (BC IV) when $\lambda=1\sim 4, j=5$.

λ	BC I		BC II		BC III		BC IV	
	$\ E_w\ _1$	$\ E_w\ _2$						
1	1.3E-07	1.3E-07	3.3E-08	2.2E-08	2.8E-06	1.9E-06	2.3E-07	1.7E-07
1.25	1.3E-07	9.4E-08	1.2E-07	9.0E-08	6.2E-06	4.8E-06	4.1E-07	3.4E-07
1.5	2.0E-07	1.7E-07	3.0E-07	2.5E-07	1.1E-05	9.4E-06	6.5E-07	5.8E-07
1.75	2.3E-07	2.1E-07	6.1E-07	5.6E-07	1.6E-05	1.5E-05	9.0E-07	8.7E-07
2	2.4E-07	2.4E-07	1.0E-06	1.0E-06	2.2E-05	2.3E-05	1.1E-06	1.2E-06
2.5	2.4E-07	2.7E-07	1.5E-06	1.7E-06	3.4E-05	4.0E-05	1.4E-06	1.7E-06
3	2.3E-07	2.8E-07	1.1E-06	1.6E-06	4.4E-05	5.8E-05	1.3E-06	1.8E-06
4	1.9E-07	2.7E-07	7.4E-07	1.5E-06	5.8E-05	9.0E-05	9.2E-07	1.7E-06

Table 6: Mean square error of convergent deflection of orthotropic plate on elastic foundation ($k_1=g_\xi=g_\eta=1, k_2=50$) with circled clamped edges by different selection of linear operators when $c_1=c_2=-35/100$.

level	$ErrSQ$	$\hat{\mathcal{L}}$	$\hat{\mathcal{L}}_1$	$\hat{\mathcal{L}}_2$	$\hat{\mathcal{L}}_3$	$\hat{\mathcal{L}}_4$
$j=4$	w	3.0E-05	2.6E-05	5.5E-07	1.2E-06	5.3E-05
	φ	1.7E-03	1.6E-03	3.6E-04	3.2E-04	2.2E-05
$j=5$	w	4.6E-05	4.1E-05	8.9E-08	5.1E-09	4.4E-05
	φ	6.1E-04	5.5E-04	5.3E-06	1.4E-06	4.3E-04
$j=6$	w	8.7E-05	4.3E-05	1.3E-07	2.4E-11	4.4E-05
	φ	3.0E-04	5.2E-04	1.5E-06	6.2E-09	4.9E-04

$\hat{\mathcal{L}}_3$ performs the best precision of deflection is around 10^{-11} but with the longest convergent time. To append linear ingredient of w in nonlinear item on the basis of $\hat{\mathcal{L}}_3, \hat{\mathcal{L}}_4$ is further calculated but with poor precision resulting in more complexity in construction of iterative matrix $\tilde{\mathbf{A}}_w$. As discussed, the linear component of original nonlinear equation can be selected as the auxiliary linear operator in the homotopy-based wavelet approach which is convenient and demonstrates superior approaching precision.

6 Concluding remarks

In the paper, a generalized homotopy-based wavelet method for nonlinear partial differential equation with nonhomogeneous boundaries is developed by means of constructing a homotopy to transform the original equation or a system of coupled equations into an infinite decoupled sequence of linear differential equations and solved by wavelet Galerkin method. Based on Taylor expansion by the improvement of boundary difference order, the accuracy of wavelet approximation is largely improved and the accumulated error at boundary is successfully suppressed in application. A unified high-precision wavelet approximation scheme is formulated for inhomogeneous boundaries including

generalized Dirichlet, Neumann, Robin and Cauchy types, which overcomes the shortcomings of accuracy loss in homogenization. Large deflection bending of orthotropic plate with forced boundary moments and rotations on nonlinear foundation is used as an example to illustrate the homotopy-based wavelet scheme, while the obtained deflection solution of plate at both small and largely deformed stage has been validated in good accuracy with published results. Compared to the other homotopy-based approach, there are some advantages within the wavelet scheme

1. Differential operations are degraded into algebra operations by converting the differential operators into approximately symmetrical iterative matrices independent of the problem to be solved greatly reducing computational complexity.
2. Nonhomogeneous edges are directly approached by boundary Coiflets as an iterative correction dispensing with homogenization by variable substitution, while the convergence can be ensured by the iteration approach.
3. The auxiliary linear operator can be determined by linear component of original nonlinear equation which is convenient and demonstrates excellent approaching precision.

While the method has been validated accurate for nonlinear nonhomogeneous boundary value problem, further work is required in order to generalise it to initial boundary value problems so as to expand broader applications.

Acknowledgements

This work is partially supported by the National Natural Science Foundation of China (Grant No. 11902189)

References

- [1] T. TANG, *The hermite spectral method for gaussian-type functions*, SIAM J. Sci. Comput., 14(3) (1993), pp. 594–606.
- [2] B. COCKBURN, G. E. KARNIADAKIS, AND C.-W. SHU, *Discontinuous Galerkin Methods: Theory, Computation and Applications*, Vol. 11, Springer Science and Business Media, 2012.
- [3] P. F. FISCHER, AND E. M. RØNQUIST, *Spectral element methods for large scale parallel Navier–Stokes calculations*, Comput. Methods Appl. Mech. Eng., 116(1-4) (1994), pp. 69–76.
- [4] K. VAN DEN ABEELE, C. LACOR, AND Z. J. WANG, *On the connection between the spectral volume and the spectral difference method*, J. Comput. Phys., 227(2) (2007), pp. 877–885.
- [5] J. VIRIEUX, *P-sv wave propagation in heterogeneous media: Velocity-stress finite-difference method*, Geophys., 51(4) (1986), pp. 889–901.
- [6] O. C. ZIENKIEWICZ, R. L. TAYLOR, P. NITHIARASU, AND J. ZHU, *The Finite Element Method*, Vol. 3, McGraw-Hill London, 1977.

- [7] J. KIM, D. KIM, AND H. CHOI, *An immersed-boundary finite-volume method for simulations of flow in complex geometries*, J. Comput. Phys., 171(1) (2001), pp. 132–150.
- [8] A. PORTELA, M. ALIABADI, AND D. ROOKE, *The dual boundary element method: effective implementation for crack problems*, Int. J. Numer. Methods Eng., 33(6) (1992), pp. 1269–1287.
- [9] S. J. LIAO, *The Proposed Homotopy Analysis Technique for the Solution of Nonlinear Problems*, Ph.D. thesis, Shanghai Jiao Tong University, (1992).
- [10] R. A. VAN GORDER, *Analytical method for the construction of solutions to the föppl–von kármán equations governing deflections of a thin flat plate*, Int. J. Non-Linear Mech., 47(3) (2012), pp. 1–6.
- [11] S. MOTSA, P. SIBANDA, AND S. SHATEYI, *A new spectral-homotopy analysis method for solving a nonlinear second order bvp*, Commun. Nonlinear Sci. Numer. Simul., 15(9) (2010), pp. 2293–2302.
- [12] S. S. MOTSA, S. SHATEYI, G. T. MAREWO, AND P. SIBANDA, *An improved spectral homotopy analysis method for mhd flow in a semi-porous channel*, Numer. Algorithms, 60(3) (2012), pp. 463–481.
- [13] A. C. CULLEN, AND S. R. CLARKE, *A fast, spectrally accurate homotopy based numerical method for solving nonlinear differential equations*, J. Comput. Phys., 385 (2019) 106–118.
- [14] J. LEWALLE, *Wavelet transforms of the navier-stokes equations and the generalized dimensions of turbulence*, Appl. Sci. Res., 51(1-2) (1993), pp. 109–113.
- [15] W. YAN, L. DEQUN, AND W. BAISUO, *Daubechies wavelet construction using homotopy method*, Chinese J. Electron., 16(1) (2007), pp. 93–96.
- [16] C. CHEN, AND C. HSIAO, *Haar wavelet method for solving lumped and distributedparameter systems*, IEEE Proceedings Control Theory Appl., 144(1) (1997), pp. 87–94.
- [17] A. GROSSMANN, AND J. MORLET, *Decomposition of hardy functions into square integrable wavelets of constant shape*, SIAM J. Math. Anal., 15(4) (1984), pp. 723–736.
- [18] K. MEYER, *Scaling hamiltonian systems*, SIAM J. Math. Anal., 15(5) (1984), pp. 877–889.
- [19] G. BEYLKIN, *On the representation of operators in bases of compactly supported wavelets*, SIAM J. Numer. Anal., 29(6) (1992), pp. 1716–1740.
- [20] D. KATEB, AND K. DROUCHE, *The stromberg wavelet and the franklin system*, IEEE Trans. Signal Process., 41(12) (1993), pp. 3562–3566.
- [21] W. SWELDENS, *The lifting scheme: A custom design construction of biorthogonal wavelets*, Appl. Comput. Harmonic Anal., 3(2) (1996), pp. 186–200.
- [22] W. SWELDENS, *The lifting scheme: A construction of second generation wavelets*, SIAM J. Math. Anal., 29(2) (1998), pp. 511–546.
- [23] O. V. VASILYEV, AND C. BOWMAN, *Second-generation wavelet collocation method for the solution of partial differential equations*, J. Comput. Phys., 165(2) (2000), pp. 660–693.
- [24] D. L. DONOHO, ET AL., *Wedgelets: Nearly minimax estimation of edges*, The Annals of Statistics, 27(3) (1999), pp. 859–897.
- [25] E. CANDÈS, L. DEMANET, D. DONOHO, AND L. YING, *Fast discrete curvelet transforms*, Multiscale Model. Simul., 5(3) (2006), pp. 861–899.
- [26] M. N. DO, AND M. VETTERLI, *The finite ridgelet transform for image representation*, IEEE Trans. Image Process., 12(1) (2003), pp. 16–28.
- [27] M. N. DO, AND M. VETTERLI, *The contourlet transform: an efficient directional multiresolution image representation*, IEEE Trans. Image Process., 14(12) (2005), pp. 2091–2106.
- [28] S. JAFFARD, *Wavelet methods for fast resolution of elliptic problems*, SIAM J. Numer. Anal., 29(4) (1992), pp. 965–986.
- [29] S. BERTOLUZZA, Y. MADAY, AND J. RAVEL, *A dynamically adaptive wavelet method for solving partial differential equations*, Comput. Methods Appl. Mech. Eng., 116(1-4) (1994), pp. 293–

- 299.
- [30] F. W. ELLIOTT JR, AND A. J. MAJDA, *A wavelet monte carlo method for turbulent diffusion with many spatial scales*, J. Comput. Phys., 113(1) (1994), pp. 82–111.
- [31] S. QIAN, AND J. WEISS, *Wavelets and the numerical solution of boundary value problems*, Appl. Math. Lett., 6(1) (1993), pp. 47–52.
- [32] C. A. MICCHELLI, Y. XU, AND Y. ZHAO, *Wavelet galerkin methods for second-kind integral equations*, J. Comput. Appl. Math., 86(1) (1997), pp. 251–270.
- [33] O. V. VASILYEV, AND N. K.-R. KEVLAHAN, *An adaptive multilevel wavelet collocation method for elliptic problems*, J. Comput. Phys., 206(2) (2005), pp. 412–431.
- [34] J.-G. HAN, W.-X. REN, AND Y. HUANG, *A spline wavelet finite-element method in structural mechanics*, Int. J. Numer. Methods Eng., 66(1) (2006), pp. 166–190.
- [35] X. LIU, Y. ZHOU, X. WANG, AND J. WANG, *A wavelet method for solving a class of nonlinear boundary value problems*, Commun. Nonlinear Sci. Numer. Simul., 18(8) (2013), pp. 1939–1948.
- [36] X. LIU, G. LIU, J. WANG, AND Y. ZHOU, *A wavelet multiresolution interpolation galerkin method for targeted local solution enrichment*, Comput. Mech., 64(4) (2019), pp. 989–1016.
- [37] X. LIU, G. LIU, J. WANG, AND Y. ZHOU, *A wavelet multiresolution interpolation galerkin method with effective treatments for discontinuity for crack growth analyses*, Eng. Fract. Mech., 225 (2020), 106836.
- [38] W. CAI, AND J. WANG, *Adaptive multiresolution collocation methods for initial-boundary value problems of nonlinear PDEs*, SIAM J. Numer. Anal., 33(3) (1996), pp. 937–970.
- [39] J. S. HESTHAVEN, AND L. M. JAMESON, *A wavelet optimized adaptive multi-domain method*, J. Comput. Phys., 145(1) (1998), pp. 280–296.
- [40] R. R. COIFMAN, Y. MEYER, S. QUAKE, AND M. V. WICKERHAUSER, *Signal processing and compression with wavelet packets*, in: Wavelets and Their Applications, Springer, 1994, pp. 363–379.
- [41] J. TIAN, *The Mathematical Theory and Applications of Biorthogonal Coifman Wavelet Systems*, Ph.D. thesis, Rice University, (1996).
- [42] D. WEI, *Coiflet-Type Wavelets: Theory, Design, and Applications*, Ph.D. thesis, University of Texas at Austin, (1998).
- [43] D. WEI, A. C. BOVIK, AND B. L. EVANS, *Generalized coiflets: a new family of orthonormal wavelets*, in: Conference Record of the Thirty-First Asilomar Conference on Signals, Systems and Computers (Cat. No. 97CB36136), Vol. 2, IEEE, 1997, pp. 1259–1263.
- [44] J.-Z. WANG, *Generalized Theory and Arithmetic of Orthogonal Wavelets and Applications to Researches of Mechanics Including Piezoelectric Smart Structures*, Lanzhou Univeristy, China.
- [45] L. ZHANG, J. WANG, X. LIU, AND Y. ZHOU, *A wavelet integral collocation method for nonlinear boundary value problems in physics*, Comput. Phys. Commun., 215 (2017), pp. 91–102.
- [46] Z. YANG, AND S. LIAO, *A ham-based wavelet approach for nonlinear ordinary differential equations*, Commun. Nonlinear Sci. Numer. Simul., 48 (2017), pp. 439–453.
- [47] Z. YANG, AND S. LIAO, *A ham-based wavelet approach for nonlinear partial differential equations: Two dimensional bratu problem as an application* Commun. Nonlinear Sci. Numer. Simul., 53 (2017), pp. 249–262.
- [48] Q. YU, H. XU, AND S. LIAO, *Coiflets solutions for föppl-von kármán equations governing large deflection of a thin flat plate by a novel wavelet-homotopy approach*, Numer. Algorithms, (2018), pp. 1–28.
- [49] Q. YU, H. XU, S. LIAO, AND Z. YANG, *A novel homotopy-wavelet approach for solving stream*

- function-vorticity formulation of navier–stokes equations*, Commun. Nonlinear Sci. Numer. Simul., 67 (2019), pp. 124–151.
- [50] Q. YU, H. XU, AND S. LIAO, *Analysis of mixed convection flow in an inclined lid-driven enclosure with buongiorno’s nanofluid model*, Int. J. Heat Mass Transf., 126 (2018), pp. 221–236.
- [51] Q. YU, *A decoupled wavelet approach for multiple physical flow fields of binary nanofluid in double-diffusive convection*, Appl. Math. Comput. 404 (2021), 126232.
- [52] S. E. KELLY, *Gibbs phenomenon for wavelets*, Appl. Comput. Harmonic Anal., 3(1) (1996), pp. 72–81.
- [53] S. QIAN, AND J. WEISS, *Wavelets and the numerical solution of partial differential equations*, J. Comput. Phys., 106(1) (1993), pp. 155–175.
- [54] S. LAZAAR, P. PONENTI, J. LIANDRAT, AND P. TCHAMITCHIAN, *Wavelet algorithms for numerical resolution of partial differential equations*, Comput. Methods Appl. Mech. Eng., 116(1-4) (1994), pp. 309–314.
- [55] C. K. CHUI, AND E. QUAK, *Wavelets on a bounded interval*, in: Numerical Methods in Approximation Theory, Vol. 9, Springer, 1992, pp. 53–75.
- [56] I. DAUBECHIES, *Two recent results on wavelets: wavelet bases for the interval, and biorthogonal wavelets diagonalizing the derivative operator*, Recent Adv. Wavelet Anal., 3 (1994), pp. 237–257.
- [57] Z. YANG, AND S. LIAO, *On the generalized wavelet-galerkin method*, J. Comput. Appl. Math., 331 (2018), pp. 178–195.
- [58] M.-Q. CHEN, C. HWANG, AND Y.-P. SHIH, *The computation of wavelet-galerkin approximation on a bounded interval*, Int. J. Numer. Methods Eng., 39 (1996), pp. 2921–2944.
- [59] A. KUTLU, AND M. H. OMURTAG, *Large deflection bending analysis of elliptic plates on orthotropic elastic foundation with mixed finite element method*, Int. J. Mech. Sci., 65(1) (2012), pp. 64–74.
- [60] S. P. TIMOSHENKO, AND S. WOINOWSKY-KRIEGER, *Theory of Plates and Shells*, McGraw-hill, 1959.
- [61] F. MBAKOGU, AND M. PAVLOVIĆ, *Bending of clamped orthotropic rectangular plates: a variational symbolic solution*, Comput. Struct., 77(2) (2000), pp. 117–128.
- [62] S. ZHANG, AND L. XU, *Bending of rectangular orthotropic thin plates with rotationally restrained edges: A finite integral transform solution*, Appl. Math. Model., 46 (2017), pp. 48–62.
- [63] L. RUI, Z. YANG, B. TIAN, AND Y. LIU, *On the finite integral transform method for exact bending solutions of fully clamped orthotropic rectangular thin plates*, Appl. Math. Lett., 22(12) (2009), pp. 1821–1827.
- [64] A. M. ZENKOUR, *An exact solution for the bending of thin rectangular plates with uniform, linear, and quadratic thickness variations*, Int. J. Mech. Sci., 45(2) (2003), pp. 295–315.